NASA TECHNICAL MEMORANDUM

NASA TM X-1267

COOLED BAFFLE DEVELOPMENT FOR M-1 ENGINE USING A SUBSCALE ROCKET ENGINE

by E. William Conrad, John P. Wanhainen, and Jerome K. Curley

Lewis Research Center
Cleveland, Obio

NATIONAL AERONAUTICS AND SPACE ADMINISTRATION • WASHINGTON, D. C. • OCTOBER 1966

NASA TM X-1267

COOLED BAFFLE DEVELOPMENT FOR M-1 ENGINE USING A SUBSCALE ROCKET ENGINE

By E. William Conrad, John P. Wanhainen, and Jerome K. Curley

Lewis Research Center
Cleveland, Ohio

NATIONAL AERONAUTICS AND SPACE ADMINISTRATION

COOLED BAFFLE DEVELOPMENT FOR M-1 ENGINE USING A SUBSCALE ROCKET ENGINE (U)

by E. William Conrad, John P. Wanhainen, and Jerome K. Curley

Lewis Research Center

SUMMARY

A subscale rocket of 15 000 pounds thrust was used to provide a realistic environment for development of a suitable cooled baffle configuration for use in the M-1 engine development program. Chamber pressure, contraction ratio, mixture ratio, and injector elements were identical with the full-scale M-1 engine. Inasmuch as the size of an individual baffle compartment of the full-scale engine was approximated by the subscale engine, the heat transfer environment of the full-scale engine was also closely simulated.

As a result of tests using a series of 25 baffles (segments of full scale) employing several cooling techniques, a configuration was developed that satisfied the design requirements and exhibited adequate durability. All baffle configurations employing transpiration cooling exhibited an unexpected multivalued flow characteristic curve, rendering these configurations unsuitable for use in the M-1 engine program.

INTRODUCTION

In the time period since 1956, virtually every rocket engine with over 10 000 pounds thrust developed in this country has been plagued with the screech problem during the development. Between 50 and 100 injectors using largely "cut and try" variations have been evaluated in each of several engine programs before a reasonable screech margin was obtained. Costs and time delays have obviously been enormous - particularly, for the larger engines. In an effort to avoid this situation, M-1 engine designers have made maximum use of recent information on injector element design from reference 1 and from the J-2 engine development program. Although the injector elements which evolved have shown adequate stability in a 15 000-pound thrust chamber, no guarantee of stability in full scale (1 500 000 lb thrust) could be given in view of a lack of scaling laws regarding

the effects of chamber diameter on screech. Accordingly, it was decided to use baffles with the M-1 injectors. For screech suppression, the baffle geometry was based upon work such as that reported in reference 2 and F-1 engine quarterly progress reports.

The problems involved in adequately cooling baffles in the M-1 engine are formidable inasmuch as the local heat flux is estimated to be as high as 20 Btu per square inch per second. Inasmuch as coolant pressure drops available ruled out regeneratively cooled baffles, transpiration, film, and convective cooling techniques were investigated. It was furthermore estimated that only 4 percent of the total hydrogen could be employed with these techniques for baffle cooling without excessive loss in specific impulse efficiency. Because the cost and time delay involved in developing adequate cooling techniques on the full-scale hardware would have been prohibitive, the subscale program discussed herein was conceived. The program was conducted at the Lewis Research Center.

The tests were accomplished by mounting 3-inch segments of the full-scale baffle on the injector of a 15 000-pound hydrogen-oxygen rocket engine and progressively reducing the hydrogen flow to the baffle test specimen until damage or failure occurred. A total of 25 configurations was tested to achieve baffle integrity at minimum hydrogen coolant flow and within the allowable (injector) pressure drop. Although the injector used was very small (5.39 in. in diam. as opposed to 42 in. for full scale), the concentric tube elements used were full scale as was the baffle length. In addition, the element density of the full-scale engine was duplicated as well as the element distances from the baffle surfaces. Testing was done at the full-scale chamber pressure of 1050 pounds per square inch. The effect of two oxidizer tube modifications (to the elements adjacent to the baffle) on heat flux to the baffle was also determined qualitatively for inclusion during the concurrent fabrication of the full-scale injectors by the engine manufacturer.

APPARATUS

Test Facility

The Rocket Engine Test Facility of the Lewis Research Center is a 50 000-pound-thrust sea level stand equipped with an exhaust gas muffler and scrubber. A sketch of the facility is shown in figure 1. The engine was mounted on the thrust stand to fire vertically into the scrubber where the exhaust gases were sprayed with water at rates to 50 000 gallons per minute for the purpose of cooling and sound suppression. The cooled exhaust gases were discharged into the atmosphere from the top of a 70-foot exhaust stack. Initially, carbon dioxide was used to inert the scrubber before and after each run to prevent explosions. Later in the program, pilot flames were installed at various locations in the scrubber to burn excess hydrogen. These burn-off jets were completely

successful and eliminated the need for the expensive and time-consuming carbon dioxide inerting operation.

The facility utilized a pressurized propellant system to deliver the propellants to the engine from the storage tanks. The oxygen propellant line was immersed in a nitrogen bath, and the liquid hydrogen line was insulated with a plastic-type foam. The propellant storage tanks consisted of 75- and 175-cubic-foot liquid hydrogen Dewars, a 120 000-standard-cubic-foot (2200-psi) gaseous hydrogen bottle rack, and a 55-cubic-foot liquid oxygen tank submerged in a liquid nitrogen bath.

The facility was operated remotely from a control room located 2000 feet from the test stand. In addition to Lewis' central data retrieval system, the facility was equipped with several direct reading oscillographs and tape recorders to record test results.

Engine

The rocket engine (fig. 2) was composed of a 52-element injector with a porous stainless steel faceplate, a 10-inch-long cylindrical combustion chamber with a 5.39-inch inside diameter, and a convergent-divergent exhaust nozzle with a contraction ratio of 1.7 to match the full-scale engine; hence, heat flux distribution near the baffle test specimen. Water cooled chambers were originally planned to achieve the desired nominal run time of 10 seconds but failed in early testing. A variety of graphite and ablative thrust chamber liners and nozzles were, therefore, used as expedient. In addition, a water cooled spray ring was sometimes used with a zirconium oxide coated mild steel nozzle. Hardware attrition was high, with most nozzles being discarded after 2 or 3 runs owing to erosion of the throat and the associated deviation from the desired chamber pressure and contraction ratio. These operational aspects are, however, not germane to the objectives of this report and will not be discussed in detail.

Injector

A view of the injector with a convectively cooled baffle specimen installed is shown in figure 3. The injector was designed to simulate the full-scale M-1 injector. The 52 individual injector elements were identical to those (3248) to be used in the M-1 engine. These elements used a hydrogen-to-oxygen velocity ratio of 21 for good screech stability on the basis of the information in reference 1. Also, based on experience from the J-2 engine development program, the oxidizer tubes were recessed 0.2 inch. Cross-sectional views of the nominal element used in the M-1 engine and two types of modified elements for use adjacent to the baffle are given in figure 4. Modifications A and B were

used separately or together as shown in figure 5 at various points in the course of the program (as denoted in table I) to reduce the heat load to the baffle through changes in the local mixture ratio adjacent to the baffle. It will be noted also in figure 5 that the oxidizer tube of the element adjacent to the end of the baffle was plugged and four holes, 0.1 inch in diameter, were drilled adjacent to the baffle corners to reduce heat load on the edge of the baffle, inasmuch as edges such as this are not present in the full-scale engine (fig. 6). To assist in reducing the erosion rate of the thrust chamber walls, 42 film cooling holes, 0.07 inch in diameter, were drilled in the injector face perimeter (fig. 6). This provided about 12 percent of the total hydrogen weight flow to act as chamber film coolant compared to about 3 percent in the final full-scale engine design. However, since this coolant was at the chamber walls, completely remote from the baffle, the only effect of the additional film cooling was to slightly increase the element oxidant-fuel ratio. The spacing of the elements with respect to the baffle was identical to the full-scale engine. The distance from the centerline of the elements to the centerline of the baffle was 0.69 inch. The injector faceplate was made of porous stainless steel rated at 300 standard cubic feet per minute at 2 pounds per square inch differential. A separately controlled and metered flow of hydrogen at a temperature close to 140° R was supplied through tubes to the base of the baffle (fig. 2). This deviates from the full-scale design in that a separate baffle cooling system will not be provided and the coolant to the baffle will be supplied from the hydrogen injector cavity through holes drilled into the faceplate.

Baffle Configuration

As noted earlier, the baffle specimens tested corresponded to nominal 3-inch segments of the full-scale M-1 baffle. The planform of the full-scale M-1 baffle shown in figure 6 was selected by the engine manufacturer on the basis of experience such as that typified in reference 2 for optimum screech suppression characteristics. Three basic techniques were evaluated in this program for baffle cooling of the test specimens: transpiration, convection, and film.

The 25 baffles tested employed one or more of these techniques, which are illustrated schematically in figure 7. Pertinent information on the injector-baffle configurations is given in table I, and additional details are given in figure 8. Baffle specimems were attached to the injector by four 3/16-inch bolts, which extended completely through the injector assembly and threaded into the lower portion of the baffle (fig. 2). Each of these bolts was surrounded by a concentric tube of larger diameter which conducted the hydrogen for baffle cooling through the injector to the base of the baffle. The joint at the injector face was sealed by the use of a Teflon O-ring in a groove concentric with each of the four annular hydrogen passages.

To eliminate the unwanted heat flux at the baffle edges, one further technique was used with many baffles as noted in table I. A strip of Refrasil-phenolic ablative material was attached to cover and protect the edge nearest the engine centerline. On one baffle, a second strip of ablative material was also installed between the baffle and the chamber wall because of excessive chamber erosion. Ablative life was adequate for the run durations involved.

Instrumentation

The instrumentation used in the investigation is given in detail and the locations for the various transducers are shown in a sketch of the engine and associated plumbing in figure 9. The signals from the transducers were transmitted to Lewis' automatic digital data recording system.

Oxygen propellant weight flow was determined with a vane-type flowmeter, which was calibrated with water using a static weighing system. The correction from water calibration to cryogenic calibration, which accounted for the dimensional change of the instrument with temperature, was obtained from the flowmeter manufacturer. Liquid hydrogen weight flow was measured using a venturi, and the gaseous hydrogen weight flow was measured using an orifice plate. The strain-gage-type pressure transducers were calibrated by comparison with a commercial standard. Hydrogen temperatures were measured by platinum resistance-type sensors. The pressure and temperature systems were calibrated immediately prior to data acquisition by an electrical two-step calibration system, which used resistances in an electrical circuit to simulate a given pressure or temperature.

PROCEDURE

Prior to an engine firing, the facility propellant lines were cooled to ensure that propellants would be delivered to the injector at the desired conditions. This was accomplished by flowing a small amount of liquid propellant through the lines and out the facility atmospheric vents. When the lines were properly cooled, a time-sequencing system was employed to control automatically the events and duration of the rocket firing. The first step in the firing sequence was a 1-second lead of liquid hydrogen for prechill prior to stepping the mixing valves to the preset condition to deliver hydrogen to the injector at a temperature of 140° R. At the same time, the baffle coolant flow and the fluorine flow (injected into the oxygen cavity for ignition) were initiated. After the oxygen fire valve

has been ramped open and chamber pressure had reached rated conditions, the fluorine flow was terminated. The baffle coolant flow was held at a constant value during the test by a commercial servo valve control system. Engine operating conditions, which were nominally a chamber pressure of 1050 pounds per square inch absolute and an oxidant-fuel ratio of 6.0, were held essentially constant throughout the program. The various baffle configurations were operated for 2 to 10 seconds at discrete points over a range of decreasing coolant flows to determine the minimum value at which the design was adequately cooled. The condition of the baffle after each test was determined by visual inspection.

RESULTS AND DISCUSSION

In keeping with the objectives of this study and the constraints imposed in the engine application, the results are presented as curves of baffle differential pressure as a function of baffle coolant flow. Engine operating conditions, propellant weight flows, and other engine parameters are presented in table II for each test. In figure 10, a typical anticipated baffle operating line is shown in relation to a design region, which is an area that encompasses variations in flow and pressure drop due to a radial pressure gradient in the hydrogen injector cavity and tolerances in porosity of available materials or fabrication dimensional tolerances.

As noted earlier, the test procedure allowed a period of 2 to 10 seconds of run time at each of the discrete points from 1 to 5 (see fig. 10) to allow stability of baffle temperature. Calculations have indicated that such short times are adequate because of the extremely high heat flux in the test installation ($\approx$20 Btu/in.^{2}/sec). A baffle having the characteristics shown with burnout well below design flow would be considered suitable in regard to performance but might not be desirable because of difficult fabrication problems. In the discussion to follow, the baffle configurations will be considered in groups based on the cooling techniques employed.

Transpiration Cooled Baffles

The first four transpiration cooled baffle specimens (specimens 1 to 4) were fabricated to identical specifications as shown in figure 8(a). The first baffle configuration which was evaluated with taper reamed oxidizer tubes (fig. 4(a)) was damaged by surface welding (pore closure) at a coolant weight flow of 0.38 pound per second. In an attempt to reduce the heat load to the baffle through changes in local oxidant-fuel ratio, the oxidizer tubes adjacent to the baffle were modified by indenting the taper reamed tube (fig. 4(b)) or

eliminating the 7° taper reaming operation (fig. 4(c)). Whereas damage occurred at a baffle weight flow of 0.38 pound per second with the standard element, both modifications allowed safe operation to a baffle coolant weight flow of 0.19 pound per second. Erosion was generally less severe on the side adjacent to the indented tubes. The remaining baffle configurations were evaluated with indented or combinations of indented and straight counterbored oxidizer tubes as indicated in table I. The experimental flow plotted against pressure drop characteristics shown in figure 11 were very surprising. It is seen that, as baffle coolant flow was reduced from maximum, the baffle pressure drop at first diminished as expected, but then increased with further reductions of flow below about 0.27 pound per second. At about 0.15 pound per second, a maximum occurred followed by a decrease again toward the origin of the plot. The scatter in the data is an indication of the variation in the porosity of the material from one piece to another. Published permeability tolerance for the material was ±30 percent.

The S-shaped flow characteristic was considered to be completely unsuitable inasmuch as operation could occur at any of three regions (A, B, or C indicated in fig. 11) for a given injector pressure drop, probably depending upon the sequence of propellant flows during the complex conditions typical of engine start transients. Baffle integrity at B was marginal, and damage occurred after the two short runs at point C, as shown in figure 12. Although the internal edges of the material were beveled in an attempt (figs. 8(a) and 13) to allow more coolant into the corners formed by the end cap, the corners were prone to damage before the surface welding (pore closure) shown in figure 12 occurred. Internal beveling of the corners was considered necessary since cross flow in the porous material amounts to only about 5 percent of the normal flow. Referring again to figure 11, the baffle pressure drop appears much too high even if the expected square law characteristic curve had been obtained; however, at the time baffles 1 to 4 were tested, the M-1 injector analysis was not complete and design pressure drop ranged from 145 to 175 pounds per square inch.

Baffle 5 was formed by machining the inside surfaces of the 0.240-inch-thick material to 0.090 inch over the portion up to 2.5 inches from the baffle tip (fig. 8(a)) and subsequently spark-discharge machining the machines surfaces to restore porosity. Otherwise, the baffle was identical to baffles 1 to 4. No data were obtained, however, because the baffle failed mechanically due to the internal pressure load.

Baffles 6 and 19 were identical, and were the same as baffles 1 to 4 except that the porosity was increased from a rating of 120 standard cubic feet per minute at 20-pounds-per-square-inch pressure drop to 120 standard cubic feet per minute at 2-pounds-per-square-inch pressure drop. This was done to reduce the overall level of pressure drop and, hopefully, to eliminate the undesirable S-shaped curve which baffles 1 to 4 had exhibited. Overall pressure level was reduced as shown in figure 14; however, again a sharp reversal occurred in the curve at a coolant flow of about 0.35 pound per second,

causing the center of the design region to be missed. It is surmised that the data shown are probably associated with the S-shaped characteristic although the second reversal at low flow and high pressure drop was not demonstrated. The post run condition of baffle 6 is shown in figure 15. Corner damage at the tip and some surface welding (pore closure) is evident also near the baffle tip.

Design analysis of the thermal stresses in thick porous material resulted in some doubt that large temperature gradients could be supported across the thickness of the material without yield, although considerable uncertainty existed regarding specific material properties. In view of the element of doubt, baffles 7, 8, and 9 were designed to a completely different concept as delineated in figure 8(b). These baffles employed two layers of thin porous material supported at 1/2- by 1/2-inch intervals by means of a central strut and a pin-and-tube arrangement to allow for differential thermal expansion. Baffles 7 and 8 were identical, using stainless steel mesh rated at 120 standard cubic feet per minute at 5-pounds-per-square-inch pressure drop for each layer. Baffle 9 was identical except that the outer layer was copper mesh rated at 360 standard cubic feet per minute at 5 pounds per square inch and the inner layer was stainless steel mesh rated at 80 standard cubic feet per minute at 5 pounds per square inch.

Results obtained are shown in figure 16. Again, as for the thick walled baffles, S-shaped curves were obtained. Although the curve for baffle 9 penetrated the design region, it must be considered nonsuitable along with baffles 7 and 8 because of uncertainty as to which of the possible operating points would be realized in a firing of the M-1 engine, as discussed earlier.

The postfire condition of baffle 7, after operation to about 60 percent of the design coolant flow, is given in figure 17. It is evident that surface melting and overheating of the stainless steel mesh had occurred in the tip region, and failure was imminent. The postfire condition of baffle 9, following operation at about 80 percent of design flow, is shown in figure 18. It is seen that the copper mesh layer was partially destroyed and the inner layer of stainless steel mesh was partly melted.

Reviewing figures 11, 14, and 16 reveals that all of the transpiration cooled baffles exhibited the undesirable S-shaped curve. Thus far, no similar data have been found in the published literature, possibly because experiments are not generally carried out to failure and the reversal point was not reached. Cold-flow tests at rated chamber pressure were made with baffle 19 (transpiration cooled), and results are compared with hot firing test data in figure 19. Data (corrected for slight deviations from nominal temperature) are shown for nonfiring operation with hydrogen temperatures of 140° and 520° R at the baffle inlet. Both sets of data yielded curves of a square law characteristic. At flow rates above the reversal point (0.35 lb/sec), the firing and nonfiring (140° R) flow characteristics were identical. The marked deviation of the firing data from the cold-flow case below 0.35 pound per second is attributed to an increase in the temperature of

the hydrogen during its passage through the porous material and may be associated with a sudden disruption of the cool boundary layer formed by the emerging coolant on the hot side of the baffle material. If one can judge on the basis of the increased pressure drop exhibited by the cold-flow curve for ambient hydrogen temperature at low coolant flow rates, the "effective" temperature of the hydrogen in the hot runs would appear to have reached values substantially above 520° R within the porous materials. To more fully understand the phenomena exhibited, an analysis was conducted and is given in the appendix.

Reverse Flow Convectively Cooled Baffles

As shown schematically in figure 8(c), the coolant entering the baffle base was conducted to the tip by passages in the center of the baffle and then redirected back toward the base in rectangular passages where it was dumped. Coolant passage area was designed to maintain a metal surface temperature of 1100° F. From the details given in figure 8(c), it is seen that an attempt was made to achieve some film cooling of the hot surface by the use of an angle-milled discharge slot at the baffle base.

Results obtained with both the nickel and copper baffles (numbers 14 and 21) are given in figure 20. Performance of the two was identical and deviated from the square law curve for constant temperature (superimposed) in the manner expected from considerations of momentum pressure drop due to coolant heating in the rectangular passages. It should be noted that, although the final design region was missed, the design objectives were achieved inasmuch as the data cross an interim design region which was in effect at the time the baffles were fabricated. Postfire condition is depicted in figure 21 after operation at about 75 percent of design coolant flow. Careful inspection shows that both were very near failure; the copper baffle (fig. 21(a)) shows a small blistered area indicative of incipient melting and the nickel baffle (fig. 21(b)) sustained some fine hairline cracks parallel to the cooling passages. Although the reverse flow baffles appeared to show promise, fabrication was rather complex; accordingly, no further efforts were made to refine this concept.

Convectively Cooled Baffles

As shown in figure 8(d), the coolant flowed axially from the base to the tip through tapered cooling passages designed to maintain the surface of the baffle below the melting point of the copper. The hydrogen then was discharged from the baffle tip into the combustion chamber. A computerized thermal analysis technique was used to prescribe the

variation of cooling passage area with length. This variation in area was accomplished by drilling (near the baffle surface) cylindrical coolant holes into which taper pins were inserted. Unfortunately, the axial distribution of combustion gas temperature and heat transfer coefficient along the length of the baffle are not known, yet these factors are dominant in achieving an optimum velocity distribution in the coolant passages. The import of this unknown environment is shown in reference 3 where convective cooling of the combustion chamber walls of a hydrogen-oxygen rocket was investigated experimentally. The design procedure used herein was to first compute a heat flux at the baffle tip using the equations of reference 4 and then to assume a linear variation from the tip to the baffle base. The heat flux was assumed to be zero at the base.

The results obtained with baffles 10, 13, and 13M are shown in figure 22. Referring to the results for baffle 10 indicates an analytical curve through the data points would pass under the design region indicating that the cooling passage area was larger than necessary. Although not shown in the figure, baffle 10 was operated with a measured coolant flow in the line leading to the baffle of 0.279 pound per second, a value within the design region. O-ring leakage (indicated by low pressure drop across the baffle) resulted in an even lower coolant flow to the test specimen. The postfire condition of baffle 10 was excellent as seen in figure 23, indicating this convectively cooled design was suitable for the intended service, although this point was not fully demonstrated.

Baffle 13 was designed with higher coolant velocities and was intended for operation in an early design region at 175-pounds-per-square-inch pressure drop. As seen in figure 22, the pressure drop was somewhat higher than desired. Postfire condition revealed damage near the baffle tip (fig. 24) after operation at about 75 percent of design flow.

The remaining convectively cooled baffle, 13M, was made from baffle 13 by machining off 1/2 inch of the tip and beveling the wall material as shown in the postfire photograph, figure 25. During the second firing at 0.248 pound per second, one taper pin was lost. Loss of this pin would reduce the coolant flow in all other passages and may have accounted for the erosion damage seen near the tip. It would appear, in summary, that satisfactory dump cooled baffles could probably be developed, but this expectation was not completely demonstrated in the tests which were made.

Film Cooled Baffles

As evidence of tip erosion accumulated during operations with the convectively cooled baffles, a school of thought developed which advocated the use of film cooling for protection of the tip region. Details of the two-piece film cooled baffles (baffles 16, 16M, and 17) which evolved are given in figures 8(e) and (f). With baffles 16 and 16M, the initial $1\frac{1}{2}$-inch piece in the lower heat flux region near the base was convectively cooled. The hy-

drogen was then accelerated to discharge at high velocity from holes (segments of circles) tangent to the remaining surface to be cooled by film cooling. Results obtained with baffle 16 are shown in figure 26. Erosion was experienced near the baffle tip after operation at design flow values; however, baffle pressure drop was less than design. Inspection of the baffle after firing revealed that the coolant discharge holes had "opened up," reducing discharge velocity and, hence, probably reducing the effectiveness of the film cooling. As may be seen by consideration of figure 8(e), maintenance of this design value of area for baffle 16 depended upon the cantilever strength of the material in the outer surface, since intrusion of the tip section eliminated cross tension support through the baffle in the region of the holes. Inasmuch as internal pressure loads apparently could not be properly counteracted by cantilever strength alone, the region between the individual cooling passages was electron beam welded to the underlying tip section to form a cross tension tie in baffle 16M. In addition, the overall length of 16M was reduced to $3\frac{1}{2}$ inches, the 1/2 inch being removed from the tip. Again erosion at the tip was experienced at design coolant flows (fig. 27), leading one to suspect the flame holding action on the baffle tip as a major factor. Inspection, however, also revealed that the electron beam welds on the side shown did not hold and allowed the coolant discharge area to increase. Although the pressure drop was increased somewhat (fig. 26), neither side received proper cooling; one side received more than half of the coolant but discharge velocity was lower than design; the other side received less than half of the coolant and tip erosion was more extensive. In addition, some coolant was undoubtedly lost as a result of the cracked welds on the baffle edge (fig. 27).

As shown in figure 8(f), baffle 17 was formed of two pieces held together by bolts recessed in holes drilled into the baffle tip. Circular coolant holes were used for strength, and much higher pressure drop was used to achieve very high coolant discharge velocity and thus determine feasibility of the film cooling technique for protecting the otherwise uncooled portion. A single data point (fig. 26) was obtained at a coolant flow about 10 percent above design. The extensive erosion shown at the baffle tip in figure 28 indicates that film cooling cannot adequately protect the $1\frac{1}{2}$-inch length near the baffle tip. It should be recalled here that dimpled injector oxidizer elements were used along one side and straight elements along the other side of the baffle as shown in figure 5. Erosion was less severe on the side adjacent to the dimpled tubes, and this evidence, as well as evidence from other runs, led to a decision to use dimpled oxidizer elements (fig. 4(b)) adjacent to the baffles in the M-1 engine.

Combined Film and Convectively Cooled Baffles

The results obtained with the film cooled baffles indicated that complete protection of the $1\frac{1}{2}$-inch-long tip section could not be readily accomplished by film cooling alone. Ac-

cordingly, baffles 18, 18M, 22, 23, and 24 incorporated a combination of film cooling and convective cooling. Referring to the details of these configurations in figures 8(g) and (h), it may be seen that convective cooling was used for the first 2 inches near the baffle base in the region of relatively low heat flux. By proportioning metering areas, the coolant flow was then divided such that two-thirds of the total discharged from circular holes at high velocity to film cool the remaining $1\frac{1}{2}$-inch length of baffle in the region of high heat flux. (At a coolant temperature of 140° R, the coolant discharge velocity was calculated to be about 400 ft/sec at a baffle weight flow of 0.3 lb/sec.) The remaining one-third of the coolant was directed through passages in the center of the baffle for convective cooling prior to discharge at the baffle tip.

Results obtained with baffles 18, 18M, and 22 are shown in figure 29. During the first run series with baffle 18 (circular symbol), operation occurred within the design region. Unexplicably, a second series of runs, made to provide additional confidence, resulted in a higher characteristic curve (square symbols). Postfire condition of baffle 18, shown in figure 30, was encouraging; only a small area of erosion occurred near the baffle tip adjacent to the thrust chamber wall. In view of both the baffle taper, the shorter length to be film cooled ($1\frac{1}{2}$ as compared to 2 in. with film cooled baffle 16 considered previously), and the minor damage sustained, it was reasoned that film cooling alone might be adequate. Accordingly, baffle 18 was modified to 18M by welding closed the holes in the baffle tip. The single data point (fig. 29) was at design flow but exhibited a higher pressure drop as expected. The more severe tip erosion resulting (fig. 31) indicated again that film cooling alone was not adequate in the tip region even with the shorter $1\frac{1}{2}$-inch length.

Baffle 22 was fabricated to be identical with baffle 18 to resolve the anomaly regarding the pressure drop-flow characteristics. Results shown in figure 29 confirm that the lower data in the design region are correct and lead one to suspect partial blockage of the coolant passages with ice or dirt during the second series with baffle 18. The postfire condition of baffle 22 was satisfactory, and accordingly this baffle design was fully adequate for use in the M-1 engine. A decision was made, however, that the M-1 baffles should be attached to the injector face by means of bolts inserted into the baffle tip rather than welding the baffles to the faceplate. This alteration necessitated further testing.

Baffles 23 and 24 (fig. 8(h)) were designed for the same coolant flow area as baffles 18 and 22. The taper of the film cooled portion was changed to provide a blunt base area on the baffle tip. This was done to allow simulation of a baffle attachment method for the M-1 engine. In baffle 23, the portion (one-third) of the coolant used for convective cooling was discharged through metering holes at the tip, one hole in each bolt head and one hole between each set of bolts. Results in figure 32 show that the flow characteristics were through the design region and were identical to those for baffle 22 as intended. Damage was restricted to the tip region only as shown by the photograph of the tip section in

figure 33 (the remainder of baffle 23 was cut off and joined to a new tip to form baffle 24). The erosion experienced was such that a reduction in convective cooling by the high thermal contact resistance between the bolt head and the copper baffle was suspected. Accordingly, the new tip which was substituted (baffle 24) was designed to eliminate the problem of contact resistance at the baffle tip and also to distribute the coolant closer to the hot surfaces.

Baffle 24 incorporated deeper simulated bolt holes with plugs at the baffle tip (fig. 8(h)). The plugs were machined with two flat sides to provide discharge holes shaped like segments of circles near the hot surfaces. In addition, two coolant discharge holes were used between each set of bolts. Results shown in figures 34 and 35 reveal that the design flow conditions were obtained and no erosion or damage had occurred. This baffle configuration was accordingly selected for incorporation in the M-1 development engine.

A schematic of the M-1 prototype baffle showing the 1/4-inch support bolts is presented in figure 8(i). The baffle incorporated a support bolt spacing twice that of baffle 24; also, the film and tip cooling orifices were increased to 0.041 inch. The baffle was evaluated with an injector that had indented tubes (fig. 4(b)) on both sides of the baffle. The total amount of firing time on the baffle was about 50 seconds. Three tests were achieved with 10-second durations. Results in figure 36 show that the pressure drop-flow characteristics were through the design region. The postfire condition of the baffle (fig. 37) reveals that a slight amount of tip erosion had occurred after a 10-second duration firing at the lower limit of baffle design cooling flow (0.25 lb/sec). Although these results indicate that a condition of marginal cooling had been encountered, the design was still considered suitable for its intended use since the damage occurred at the lower limit of design cooling flow. Figure 38 shows the baffle after 10 seconds of operation at 80 percent of the lower limit of design cooling flow. Considerably more tip erosion was sustained in the center of the specimen; however, it appeared that the baffle had eroded to an equilibrium heat transfer condition and therefore, could have maintained its integrity for continued operation under these conditions. The bolts and seals used in the investigation were designed to full-scale engine specifications and were found to have adequate structural integrity.

SUMMARY OF RESULTS

An experimental program was conducted at the Lewis Research Center to develop a cooled injector face baffle for use in the full-scale M-1 engine. A total of 25 baffles (3-in. segments of full scale) employing techniques of transpiration, film, and convective cooling were investigated in a subscale rocket of 15 000 pounds of thrust. The following results were obtained:

1. A subscale baffle configuration employing combined film and convective cooling techniques was developed which satisfied the design requirements and exhibited adequate durability for use in the M-1 engine development program.

2. All baffles of transpiration cooled configurations exhibited an unexpected S-shaped flow characteristic curve, rendering these configurations unsuitable for use in the M-1 engine program.

3. Baffles employing dump cooling showed promise but their suitability was not adequately demonstrated.

4. Film cooling alone was not adequate to protect the tip region of the baffle against erosion, even when only the downstream $1\frac{1}{2}$ inches were so cooled.

5. The reverse flow convectively cooled baffles satisfied the design cooling requirements; however, fabrication was complex, thus they were not considered for use in the M-1 engine.

Lewis Research Center,
National Aeronautics and Space Administration,
Cleveland, Ohio, April 5, 1966.

APPENDIX - ANALYSIS OF FLOW THROUGH POROUS MATERIAL

Since a satisfactory explanation for the S-shaped flow characteristic curve (fig. 11) could not be found in the literature, a simple analysis was conducted to determine if the deviation of the results from a square law characteristic could be attributed to an increase in the temperature of the porous media. In reference 5 an equation has been derived for porous materials which relates pressure drop, mass flow, metal hot side temperature, and the porous material configuration as follows:

$$\frac{P_1^2 - P_2^2}{L} = \alpha\left(\frac{24\ RT_m u}{Mg}\right)G + \left(\beta + \frac{1}{L}\ln\frac{P_1}{P_2}\right)\left(\frac{288\ RT_m}{Mg}\right)G^2$$

where

G weight flow rate, $lb_m/(sq\ in.)(sec)$

g gravitational conversion factor, $(lb_m)(ft)/(lb_f)(sec^2)$

L thickness of porous material, in.

M molecular weight of coolant, $lb_m/lb\ mole$

P pressure, psia

R universal gas constant, $(lb_f)(ft^3)/(in.^2)(lb\ mole)(^oR)$

T_m metal temperature (assumed equal to exit coolant temperature), ^oR

u viscosity, $lb_m/(sec)(ft)$

α viscous coefficient, $in.^{-2}$

β inertial coefficient, $in.^{-1}$

In figure 39, the measured values of baffle pressure drop plotted against coolant flow are reproduced from figure 11. Substitution of these measured quantities into the previous equation along with known gas properties and material properties (α and β are determined from information supplied by manufacturers) allows solution for the hot-side metal temperature T_m, which has been superimposed on figure 39. At coolant mass flow rates above 0.27 pound per second, the analysis indicates that the metal temperature was essentially constant. However, below about 0.27 pound per second, the computed metal temperature suddenly rises to a predicted value of 1680^o F at a coolant flow of 0.20 pound per second. Extrapolation of this curve indicates that surface melting should occur at a slightly lower coolant flow of about 0.16 pound per second. The baffle was not operated at exactly this weight flow; however, the fact that incipient melting did occur at a slightly

lower baffle weight flow of about 0.12 pound per second lends confidence to the predicted temperature curve. The equation used was similarly tested using the two sets of cold flow data shown in figure 19. This was done by substituting for T_m the coolant gas temperature (519° and 140° R) along with the measured values of baffle pressure drop and solving for coolant weight flow. Excellent agreement between the measured and calculated values of coolant weight flows was obtained.

Referring again to figure 39 reveals that, below 0.27 pound per second of coolant flow, the metal temperature suddenly rises causing the baffle pressure drop to increase. It would seem that the only reasonable explanation for the sudden increase in metal temperature must be a commensurate increase in heat flux to the baffle by convection, implying the disruption of the coolant film which apparently insulated the baffle at higher coolant flows. Obviously as coolant flow is reduced below 0.16 pound per second, the pressure drop must maximize and then decrease toward the origin, resulting in the S-shape noted.

REFERENCES

1. Wanhainen, John P.; Parish, Harold C.; and Conrad, E. William: Effect of Propellant Injection Velocity on Screech in 20 000-Pound Hydrogen-Oxygen Rocket. NASA TN D-3373, 1966.

2. Hefner, R. J.: Review of Combustion Stability Development with Storable Propellants. Paper No. 65-614, AIAA, 1965.

3. Pavli, Albert J.; Curley, Jerome K.; Masters, Philip A.; and Schwartz, R. M.: Design and Cooling Performance of a Dump-Cooled Rocket Engine. NASA TN D-3532, 1966.

4. Bartz, D. R.: A Simple Equation for Rapid Estimation of Rocket Nozzle Convective Heat Transfer Coefficients. Jet Prop., vol. 27, no. 1, Jan. 1957, pp. 49-51.

5. Green, Leon, Jr.: Fluid Flow Through Porous Metals. Rept. No. 4-111, Jet Prop. Lab., C.I.T., Aug. 19, 1949.

TABLE I. - BAFFLE CONFIGURATIONS

Baffle	Cooling method	Location of baffle details	Baffle material	Number of holes	Total hole area, $in.^2$	Total porosity, SCFM at psi/ft^2	Baffle length, in.	Injector					Ablative edge strips
								Hydrogen injection area, $in.^2$	Oxygen injection area, $in.^2$	Element type (see fig. 4)			
										Standard	Modification A	Modification B	
1	Transpiration	Fig. 8(a)	Stainless 347	--	-------	120 at 20	4.0	1.277	2.646	Yes	No	No	No
2	↓	↓	↓	--	-------	↓	↓	1.287	2.646	No	No	Yes	Yes
2				--	-------			1.277	2.327	↓	Yes	No	No
3				--	-------			1.304	2.646		No	Yes	Yes
3				--	-------			↓	2.415		Yes	↓	↓
4				--	-------	↓			↓		↓		
5				--	-------								
6		↓		--	-------	120 at 2							
7		Fig. 8(b)		--	-------	(a)		1.277	2.327			No	No
7		↓	↓	--	-------	(a)		1.304	2.415			Yes	Yes
8				--	-------	(a)		↓	↓			↓	↓
9			Copper-stainless 347	--	-------	(b)							
9	↓	↓	Copper-stainless 347	--	-------	(b)		↓	↓	↓	↓	↓	↓
10	Convective	Fig. 8(d)	Copper	22	0.110	--------		1.277	2.646	Yes	No	No	No
13	↓	Fig. 8(d)	↓	--	.03978	--------	↓	1.304	2.415	No	Yes	Yes	Yes
13M		Fig. 8(d)		--	.03978	--------	3.5	↓	↓	↓	↓	↓	↓
14		Fig. 8(c)		--	-------	--------	4.0						
16	Film	Fig. 8(e)		26	.0457	--------	4.0						
16M	Film	Fig. 8(e)		26	.0457	--------	3.5						
17	Film	Fig. 8(f)		26	.02624	--------	↓						
18	Convective and film	Fig. 8(g)		39	.04901	--------							
18M	Film	Fig. 8(g)	↓	26	.03267	--------							
19	Transpiration	Fig. 8(a)	Stainless 347	--	-------	120 at 2	4.0						
20	Convective	--------	Copper-nickel	22	.07018	--------	3.5						
21	Convective	Fig. 8(c)	Nickel	--	-------	--------							
22	Convective and film	Fig. 8(g)	Copper	39	.0491	--------							
23	↓	Fig. 8(h)	↓	33	.04930	--------							
24		Fig. 8(h)		40	.049	--------							
25		Fig. 8(i)		40	.0528	--------	↓	↓	↓	↓	↓	↓	↓

[a] Two layers; 120 at 5.

[b] Two layers; 360 at 5 and 80 at 5.

TABLE II. - M-1 BAFFLE TEST RESULTS

Test	Baffle	Location of element details in figure -			Number of elements	Liquid oxygen injection area, $in.^2$	Hydrogen injection area, $in.^2$	Chamber pressure, P_c, psia	Overall oxidant-fuel ratio	Element oxidant-fuel ratio	Oxygen injection differential pressure, psi	Hydrogen injection differential pressure, psi	Hydrogen injector temperature, ^oR	Oxygen flow, lb/sec	Hydrogen flow, lb/sec	Baffle flow, lb/sec	Measured baffle differential pressure, psi	Baffle differential pressure at 140° R, psi	Baffle inlet temperature, ^oR	Run length, sec
		4(a)	4(b)	4(c)																
176	10	Yes	No	No	52	2.646	1.1076	1035	5.6	6.9	328.5	164.3	137.2	49.10	8.11	0.526	103.0	110.8	132.2	0.66
177	10	↓	↓	↓	↓	↓	↓	1069	5.3	6.4	302.1	171.9	135.2	46.91	8.44	.279	-----	-----	149.8	.86
178	10							1079	4.5	5.5	295.5	189.7	125.5	45.92	9.55	.637	171.6	180.4	134.6	.84
193	1							1110	4.1	4.9	272.0	177.6	131.4	43.73	10.36	.381	318.1	202.3	153.7	6.59
268	10							1141	4.2	5.1	288.5	286.4	112.8	45.72	10.27	.605	-----	-----	129.0	10
274	2	No		Yes		2.327		1086	4.4	5.3	312.0	147.3	124.7	46.01	9.94	.359	323.3	249.3	140.0	10.08
275	2							1055	5.4	6.4	335.4	114.9	127.0	47.87	8.52	.278	308.6	244.9	144.1	10.1
279	7							1102	4.9	5.9	325.0	129.8	127.4	46.89	9.05	.433	-----	-----	134.7	10.13
280	7							1056	5.0	6.1	378.5	117.8	119.8	47.14	8.90	.440	245.5	157.3	135.7	10.18
281	2		Yes	No		2.646		1053	4.4	5.2	358.0	173.0	121.9	49.53	10.91	.339	337.9	260.8	142.7	4.28
295	3							1101	5.1	6.2	322.0	141.3	149.0	47.77	8.98	.338	330.3	218.7	156.6	2.02
296	↓							1089	5.5	6.8	336.2	114.6	138.4	48.76	8.41	.330	310.8	205.6	155.8	10.00
297								1089	5.6	6.9	343.0	102.9	135.0	47.81	8.09	.330	383.4	300.9	144.8	2.01
298								1004	4.5	5.4	458.2	-----	80.0	45.90	9.83	.338	405.8	310.7	147.6	6.15
301	4			Yes		2.415		1075	5.9	7.2	337.7	100.6	125.6	48.84	7.88	.287	271.2	180.7	155.3	-----
302								1096	5.5	6.6	351.2	103.3	117.0	48.90	8.61	.263	230.1	150.4	157.2	-----
303								1051	5.8	7.0	376.5	104.5	127.5	49.22	8.23	.114	370.9	301.1	158.3	.90
304	↓							1032	6.0	7.2	368	107	135	50.00	8.15	.092	349	287	158	.58
305	3							1045	5.5	6.7	361.0	124.7	137.2	49.98	8.74	.190	392.4	310.3	156.3	.83
307								1061	5.1	6.2	345.2	125.7	125.8	48.12	9.13	.231	275.4	202.5	154.4	4.3
312								1042	5.5	6.7	373.0	114.2	135.0	49.85	8.74	.237	253.8	184.4	153.0	.53
313								1062	5.3	6.3	356.8	116.2	131.4	49.01	9.02	.226	347.2	268.1	154.1	2.04
314								1069	4.9	6.0	349.6	121.6	128.8	48.87	9.57	.239	382.6	295.5	154.3	2.02
315								1056	5.1	6.2	335.4	126.8	130.0	49.37	9.25	.302	365.2	269.4	152.4	2.05
316	↓							1047	5.1	6.1	327.4	116.8	125.0	48.81	9.33	.189	416.1	340.9	152.9	.96
338	6							1087	4.9	5.9	341.9	111.5	121.9	48.41	9.65	.170	417.4	348.0	152.2	.83
342								1081	4.8	5.9	338.7	163.4	175.5	47.10	9.27	.452	-----	-----	145.6	.66
343								1056	5.3	6.6	359.6	87.7	114.5	48.23	8.56	.465	-----	-----	140.3	1.86
344								1038	5.6	6.9	359.0	83.4	124.1	49.30	8.30	.428	-----	-----	146.4	1.88
345	↓	↓	↓	↓	↓	↓	↓	1036	6.1	7.5	318.6	79.8	122.3	50.64	7.91	.377	-----	-----	145.8	1.92

TABLE II. - Continued. M-1 BAFFLE TEST RESULTS

Test	Baffle	Location of element details in figure -			Number of elements	Liquid oxygen injection area, $in.^2$	Hydrogen injection area, $in.^2$	Chamber pressure, P_c, psia	Overall oxidant-fuel ratio	Element oxidant-fuel ratio	Oxygen injection differential pressure, psi	Hydrogen injection differential pressure, psi	Hydrogen injector temperature, ^oR	Oxygen flow, lb/sec	Hydrogen flow, lb/sec	Baffle flow, lb/sec	Measured baffle differential pressure, psi	Baffle differential pressure at 140^o R, psi	Baffle inlet temperature, ^oR	Run length, sec
		4(a)	4(b)	4(c)																
346	6	No	Yes	Yes	52	2.415	1.1076	1074	4.8	5.9	349.6	160.2	157.4	48.39	9.54	.390	169.9	164.9	143.3	1.91
347								1051	5.2	6.2	357.7	126.6	143.9	49.12	9.24	.170	503.7	448.8	153.5	.88
348								1025	5.6	6.9	377.3	112.1	138.0	50.03	8.53	.273	267.0	225.2	160.6	1.95
349								1024	5.5	6.8	380.1	109.6	133.3	50.37	8.71	.335	200.2	177.5	154.1	1.85
350								1001	5.8	7.1	395.0	102.6	130.8	51.34	8.40	.340	173.8	158.0	151.0	1.89
351								988	6.1	7.6	410.8	100.2	135.3	52.18	8.07	.437	216.7	206.5	145.4	1.91
352								943	6.6	8.1	436.4	93.0	136.8	53.92	7.78	.350	152.8	144.2	146.5	5.11
353	9							996	4.5	5.5	397.7	162.1	128.1	51.30	10.81	.394	243.9	225.2	149.1	1.89
354	9							960	5.4	6.6	425.5	134.6	134.7	52.89	9.37	.260	82.5	77.1	147.6	1.83
355	9							975	5.0	6.0	416.5	140.1	125.3	52.50	10.25	.192	559.0	499.4	153.2	1.91
356	7							1074	4.4	5.3	343.1	154.1	136.2	47.85	10.52	.331	325.9	290.9	153.3	1.88
357								1041	5.3	6.5	372.6	132.8	142.9	49.84	9.01	.265	221.0	201.5	150.6	1.86
358								958	7.0	8.5	433.3	108.8	160.2	52.38	7.24	.211	238.6	219.0	149.8	1.94
359								995	5.4	6.6	388.2	116.7	125.1	50.34	8.97	.205	177.3	165.7	147.7	1.82
360								1022	4.7	5.6	362.9	126.3	109.2	49.34	10.30	.169	108.8	101.8	147.5	1.88
361								1024	4.7	5.6	373.8	120.7	108.2	49.41	10.36	.143	74.4	67.7	150.9	1.89
363	14							1128	3.9	4.7	320.5	139.4	114.3	46.22	11.47	.295	181.2	166.1	150.0	1.88
364	14							1087	4.9	5.9	342.0	102.0	111.1	47.67	9.49	.233	129.6	119.9	148.8	1.86
367	14							960	7.0	8.5	403.6	88.0	134.8	52.09	7.16	.207	106.1	99.0	147.8	4.89
368	8							988	6.4	7.9	410.2	117.1	157.9	52.19	7.74	.328	266.4	259.0	143.1	1.94
369								997	6.0	7.3	406.9	121.7	143.6	52.01	8.36	.248	214.0	205.2	144.7	1.92
370								1008	5.5	6.7	397.4	125.4	136.4	51.64	9.01	.395	129.1	124.5	144.0	1.94
371								984	6.0	7.3	420.8	118.7	139.2	52.83	8.46	.212	249.4	232.3	148.0	1.93
372								978	5.5	6.7	400.0	119.3	130.8	51.64	8.98	.372	124.4	121.6	142.5	1.92
373								945	6.1	7.3	429.3	99.4	124.8	54.22	8.67	.194	230.4	219.4	145.5	5.21
374	5							1078	5.3	6.5	352.4	132.2	159.2	48.26	8.68	.290	282.9	261.2	149.1	1.91
375	5							1072	4.9	5.9	351.7	122.3	126.3	49.22	9.75	.233	593.8	563.4	145.9	5.24
385	16							866	6.5	8.0	537.9	113.6	118.4	58.56	8.56	.327	41.5	38.4	148.9	1.96
386	16							806	6.2	7.5	528.6	135.0	125.4	57.23	8.94	.273	11.0	8.8	168.1	1.98
387	16M							1050	6.6	8.0	432.8	82.6	120.7	52.77	7.70	.297	65.3	61.7	146.4	5.10
388	16M							1038	5.8	7.0	430.6	113.5	137.5	52.56	8.73	.253	30.4	28.0	149.5	5.13
389	17							1060	5.3	6.5	411.9	137.9	151.2	51.61	9.33	.313	575.6	504.9	155.5	5.04
390	13							1003	5.9	7.1	447.9	122.8	141.7	53.61	8.78	.275	258.4	234.2	151.4	5.14
391	13							906	6.3	7.6	478.0	114.7	144.1	52.11	7.97	.227	189.6	169.5	153.1	5.05
392A	13							1052	6.7	8.1	430.3	95.9	142.8	53.03	7.65	.199	137.8	120.6	155.8	5.05
393	18							1064	6.1	7.6	426.4	119.7	165.5	51.54	7.98	.354	162.5	148.6	150.3	3.15
394								1039	6.5	7.9	438.7	109.6	153.7	53.43	7.87	.294	81.6	74.6	150.3	2.50
395								1003	6.1	7.4	466.3	89.2	107.8	55.03	8.75	.269	118.2	88.9	149.4	4.87
397A								966	6.3	7.8	469.7	109.0	138.1	55.40	8.27	.420	369.6	355.7	143.6	4.70
397B								952	6.1	7.5	486.1	115.4	134.7	56.11	8.79	.295	157.0	158.1	139.3	4.70

TABLE II. - Concluded. M-1 BAFFLE TEST RESULTS

Test	Baffle	Location of element details in figure -			Number of elements	Liquid oxygen injection area, $in.^2$	Hydrogen injection area, $in.^2$	Chamber pressure, P_c, psia	Overall oxidant-fuel ratio	Element oxidant-fuel ratio	Oxygen injection differential pressure, psi	Hydrogen injection differential pressure, psi	Hydrogen injector temperature, ^oR	Oxygen flow, lb/sec	Hydrogen flow, lb/sec	Baffle flow, lb/sec	Measured baffle differential pressure, psi	Baffle differential pressure at 140^o R, psi	Baffle inlet temperature, ^oR	Run length, sec
		4(a)	4(b)	4(c)																
398	18	No	Yes	Yes	52	2.415	1.1076	909	6.2	7.5	508.6	146.6	150.7	57.25	8.87	0.250	100.1	95.7	145.0	4.99
399	18M							1054	5.7	6.9	418.0	122.6	150.6	51.70	8.77	.258	235.8	224.5	145.5	5.01
400	13M							999	5.7	6.9	465.4	113.3	135.1	52.30	8.82	.302	380.7	365.8	144.4	4.98
401	13M							962	6.4	7.8	476.9	121.3	151.9	55.31	8.28	.248	-----	-----	141.0	4.99
402A	19							1071	5.7	7.2	412.5	93.3	126.4	51.85	8.40	.548	301.7	264.4	134.1	4.95
402B	↓							1057	6.8	8.5	424.8	86.9	152.1	51.70	7.15	.423	209.8	162.6	147.7	4.95
403								983	6.9	8.5	483.1	96.5	137.7	56.41	7.75	.357	155.8	124.1	144.6	5.04
404								959	6.7	8.3	489.0	91.7	124.9	56.23	7.95	.346	159.6	130.6	141.6	1.92
436	20							1062	6.2	7.6	412.2	110.7	144.6	52.03	7.99	.363	43.9	47.9	131.0	4.92
437	20							1020	6.8	8.3	441.8	92.3	143.9	54.48	7.72	.278	-----	-----	142.0	4.86
438	19							1058	6.0	7.1	422.1	107.2	150.5	52.38	8.56	.135	560.8	482.4	158.0	1.00
439	↓							1030	5.9	7.1	441.0	119.0	138.2	53.83	8.92	.192	561.1	484.5	157.5	4.79
440								948	7.1	8.7	488.9	101.0	143.2	56.17	7.56	.287	261.3	234.5	152.6	4.92
441								933	6.9	8.4	502.8	96.9	129.5	57.23	7.96	.269	257.2	233.0	151.4	5.02
442	23							1059	6.3	7.8	430.0	105.6	153.2	52.81	7.95	.333	163.0	142.9	155.6	4.99
443	23							1023	6.1	7.4	455.7	115.4	144.8	54.22	8.60	.290	109.7	97.4	153.9	4.95
444	23							959	6.6	8.0	488.0	96.7	129.9	56.02	8.15	.256	65.9	59.7	151.4	5.03
445	21							1061	5.9	7.2	423.0	101.8	132.5	52.55	8.58	.292	180.7	154.8	158.5	4.96
446	21							1008	6.8	8.3	466.7	96.2	144.0	55.56	7.84	.231	153.7	124.6	164.9	4.91
447	21							961	6.7	8.1	477.3	92.1	126.9	55.25	7.95	.195	120.7	100.9	161.8	4.89
448	22							1084	6.3	7.7	406.2	99.1	146.5	51.75	7.86	.347	156.1	141.9	151.0	1.91
449	22							1082	6.3	7.7	420.3	99.2	146.6	52.46	7.98	.305	103.7	90.3	156.4	1.96
450	22							1060	6.3	7.6	431.7	98.3	134.3	53.70	8.21	.269	53.6	50.0	147.8	4.98
455	24							1061	6.1	7.4	423.2	116.4	154.1	52.60	8.31	.314	123.0	119.5	143.2	4.94
456	24							1021	6.3	7.7	453.5	116.2	153.8	54.19	8.21	.272	82.0	78.6	144.7	4.90
457	24			↓	↓	↓		973	6.9	8.4	490.9	105.6	143.7	56.46	7.90	.250	63.1	61.4	143.0	4.88
508	25			No	(a)	2.503		1187	4.9	5.7	356.0	153.1	135.0	50.05	10.16	.321	177.1	164.3	148.5	2.12
509								1137	6.6	8.0	394.2	111.7	144.4	55.07	8.03	.290	169.1	159.0	146.9	2.04
510								1144	5.2	6.3	374.5	136.4	124.6	53.58	9.92	.321	183.2	182.8	140.3	10.18
511							↓	1067	6.0	7.3	404.5	150.9	154.2	55.54	8.84	.282	118.4	119.5	139.0	9.62
522							1.108	1154	5.2	6.5	368.5	139.0	144.8	52.37	9.57	.349	133.3	137.6	136.6	2.04
523								1117	5.8	7.2	379.2	116.4	136.9	53.41	8.78	.363	148.0	150.5	138.2	2.09
524								1110	5.8	7.1	391.9	116.5	131.5	54.25	9.01	.333	116.8	118.4	138.5	2.08
525								1060	5.7	7.1	416.1	145.4	127.8	53.66	8.95	.326	141.0	146.2	136.1	2.10
526								1116	6.1	7.5	383.0	122.4	153.9	53.60	8.40	.294	90.2	93.0	136.7	2.11
527								1103	6.2	7.6	397.7	118.3	145.1	54.43	8.48	.269	71.3	73.9	136.2	2.05
528								1094	6.1	7.4	400.0	114.6	133.8	54.87	8.73	.239	36.1	37.4	136.1	2.12
533	↓	↓	↓	↓	↓	↓	↓	1013	6.2	7.6	362.8	90.93	165.9	58.67	9.17	.190	-----	-----	132.6	10.17

[a] 51 for O_2 (52 for H_2).

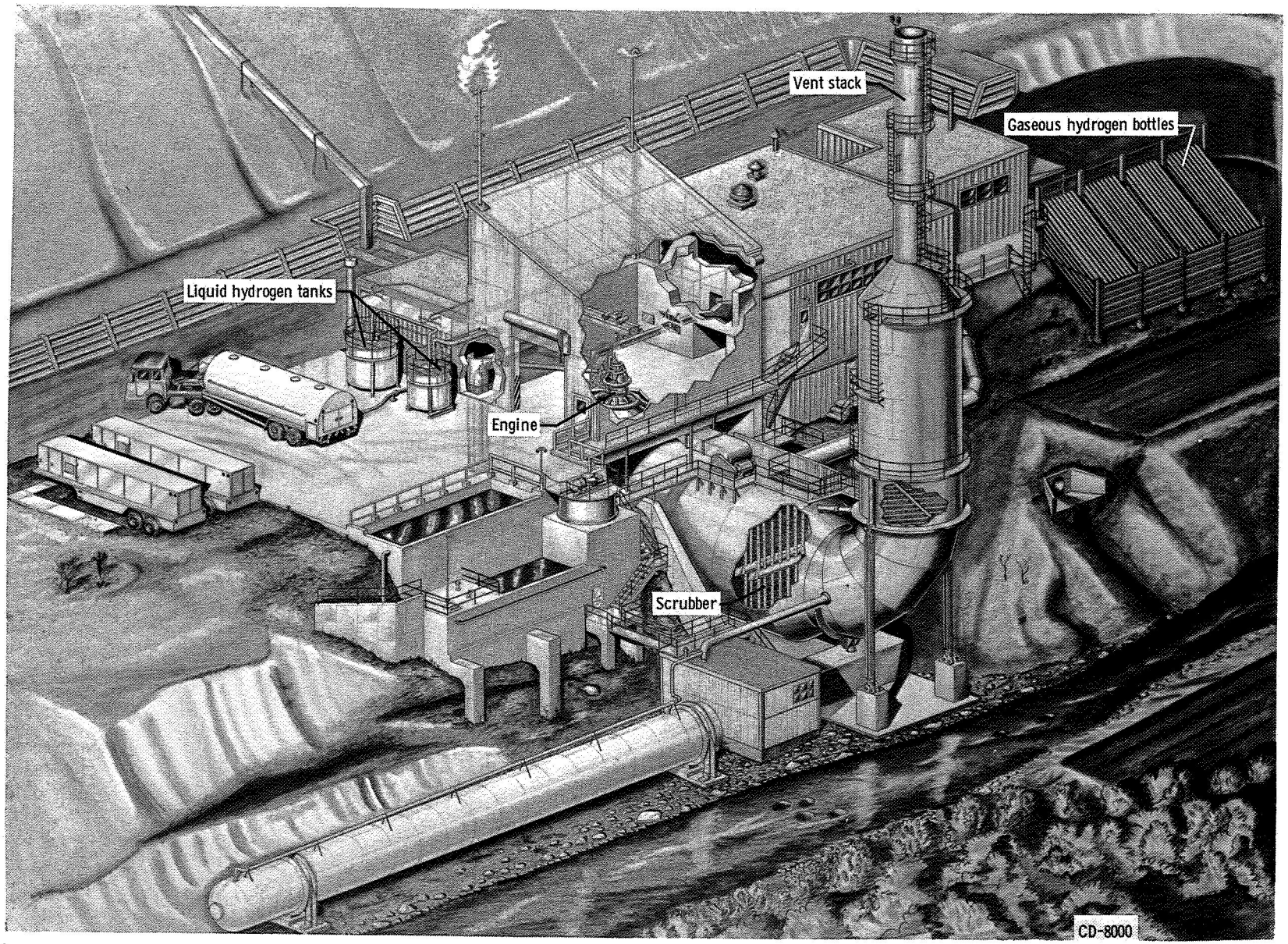

Figure 1. - Rocket engine test facility.

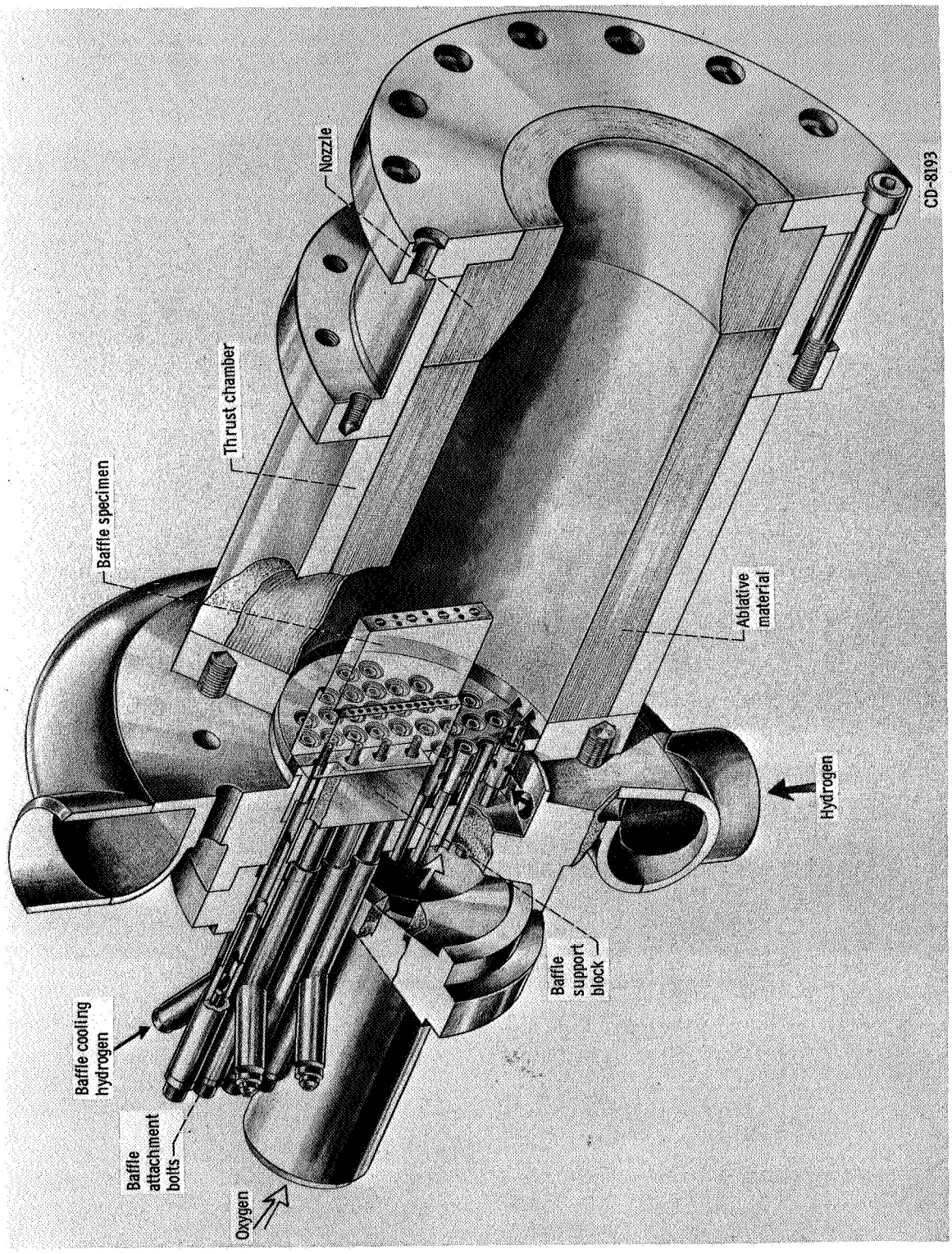

Figure 2. - Sectional view of engine.

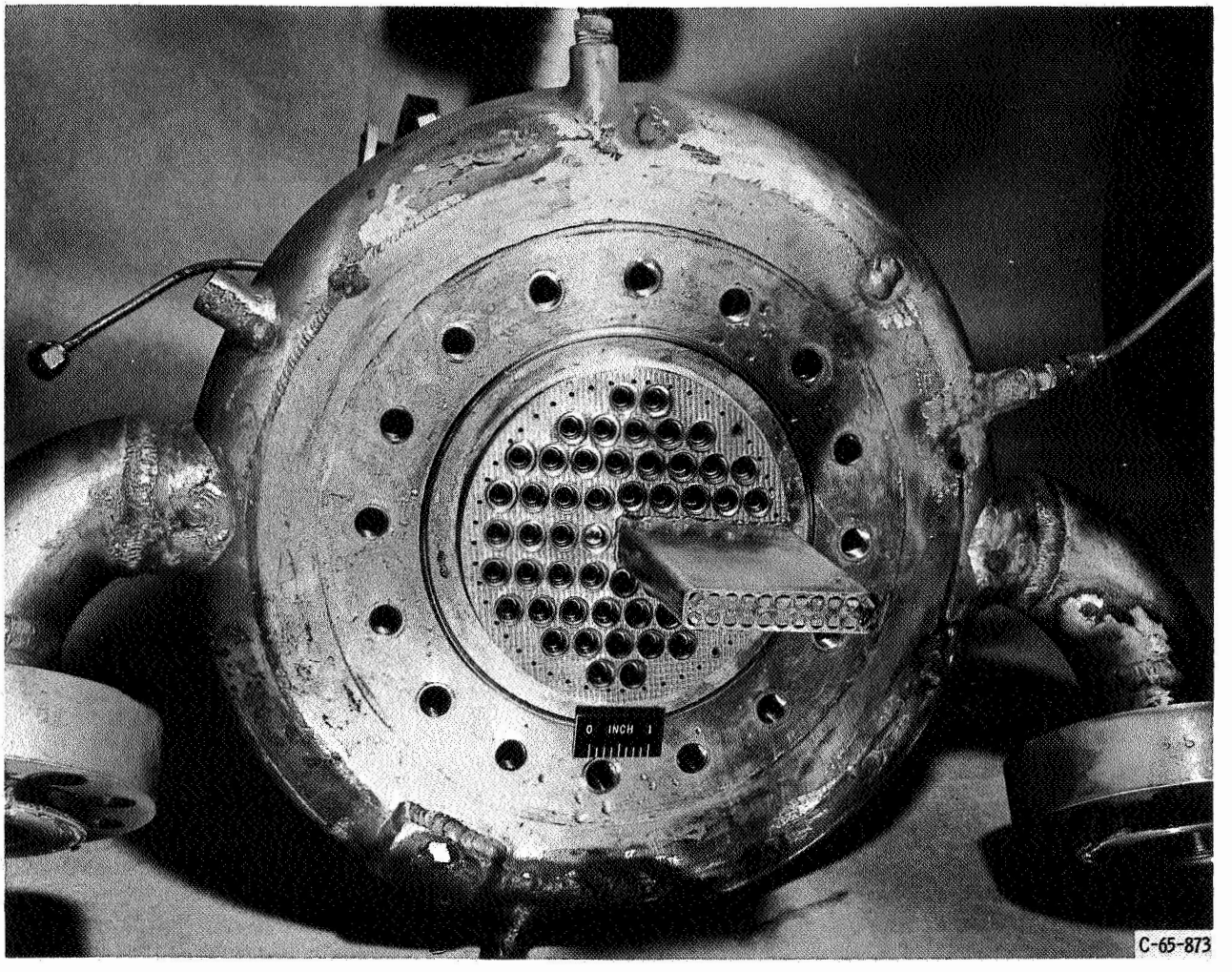

Figure 3. - View of injector with convectively cooled baffle specimen installed.

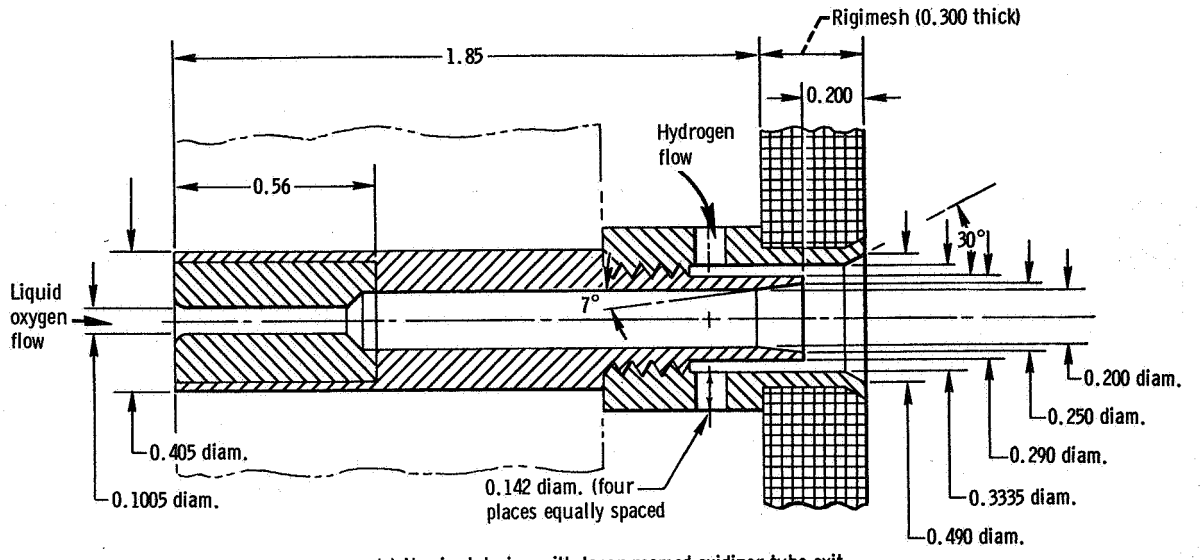

(a) Nominal design with taper reamed oxidizer tube exit.

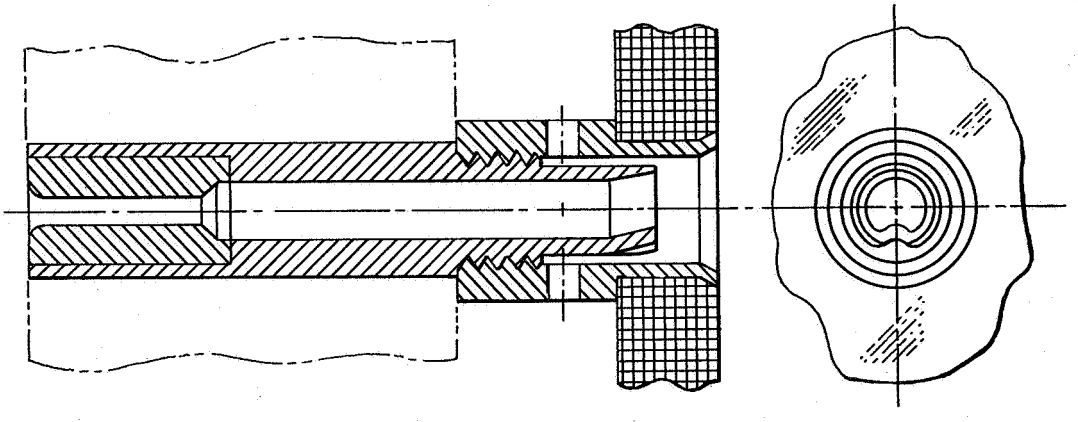

(b) Modification A - oxidizer tube with exit taper reamed and indented.

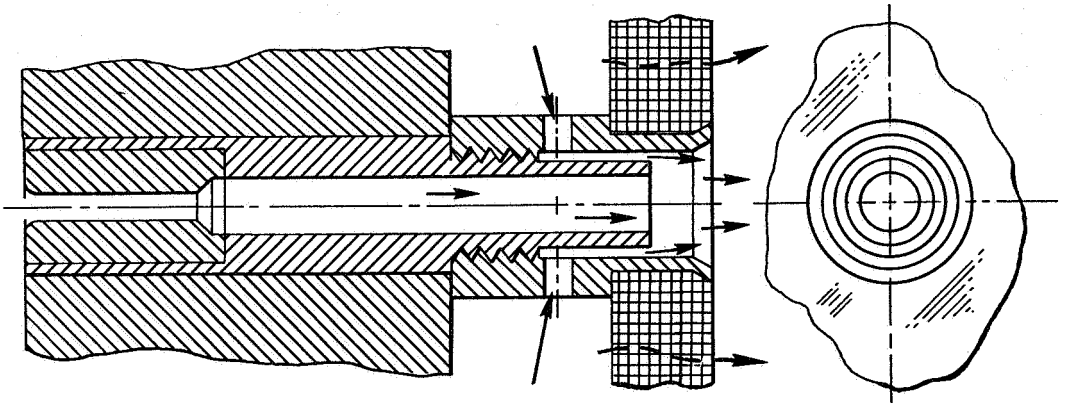

(c) Modification B - oxidizer tubes without tapered exit.

Figure 4. - Cross-sectional view of injector elements. (All dimensions are in inches unless otherwise noted.) CD-8450

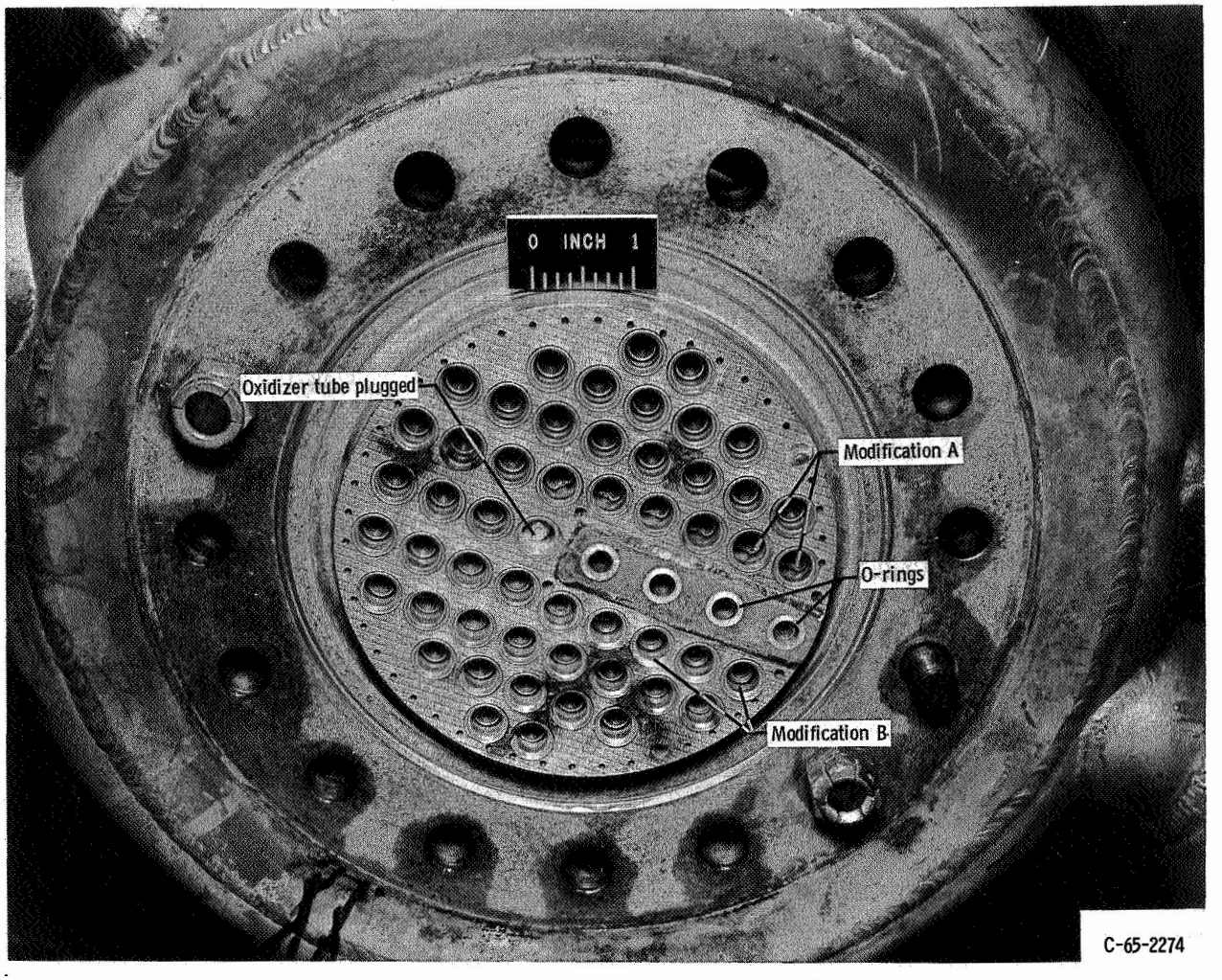

Figure 5. - View of injector showing plugged tube and relation of modified tubes A and B with respect to baffle.

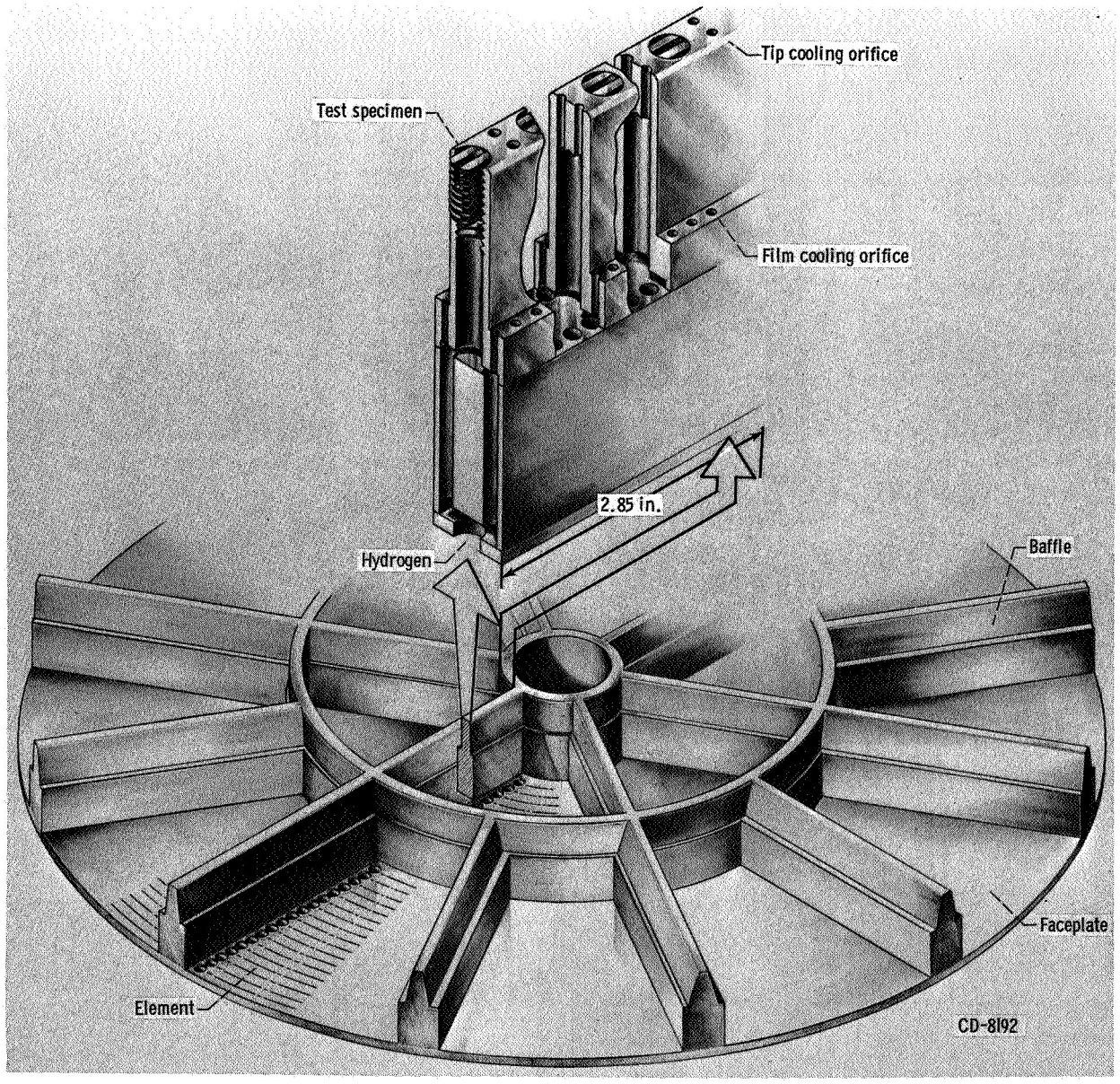

Figure 6. - Layout of full-scale M-1 engine baffle.

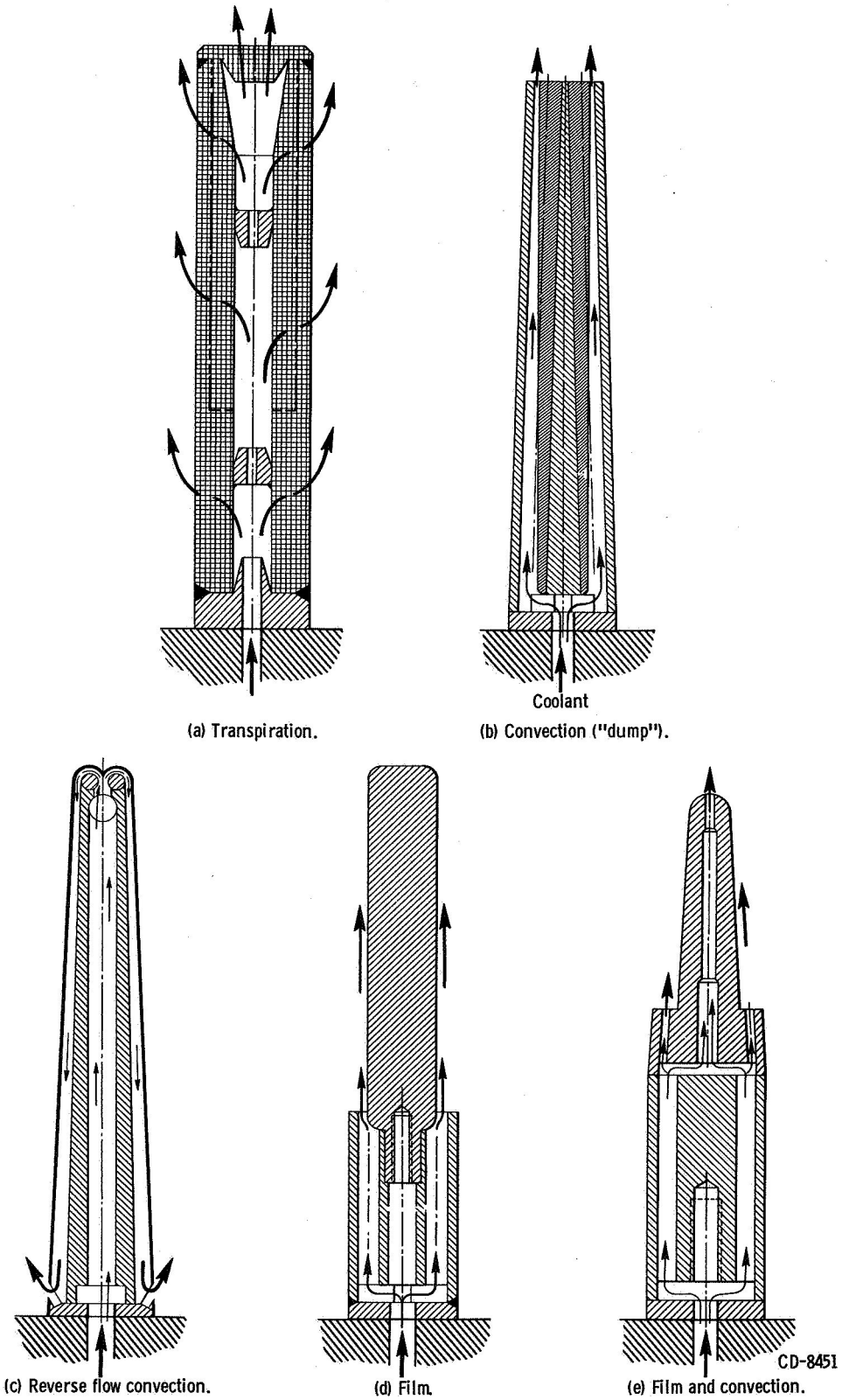

(a) Transpiration.

(b) Convection ("dump").

(c) Reverse flow convection.

(d) Film.

(e) Film and convection.

Figure 7. - Baffle cooling concepts investigated.

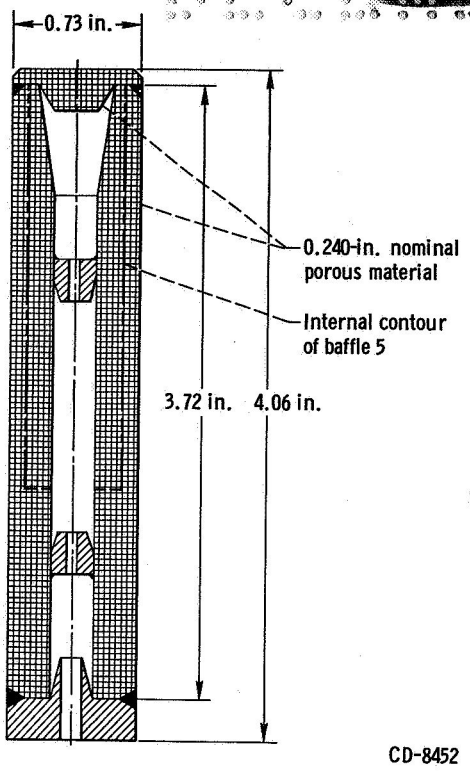

(a) Transpiration cooled; baffles 1, 2, 3, 4, 6, and 19.

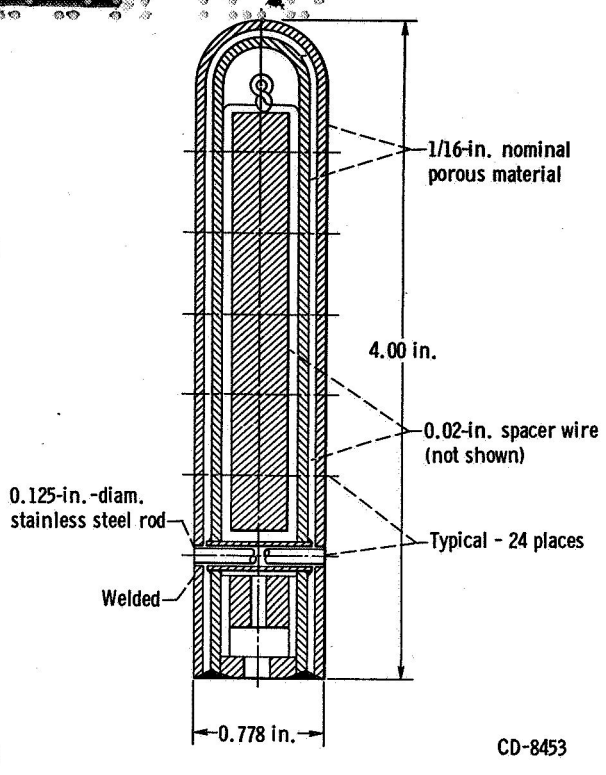

(b) Transpiration cooled - two layers; baffles 7, 8, and 9.

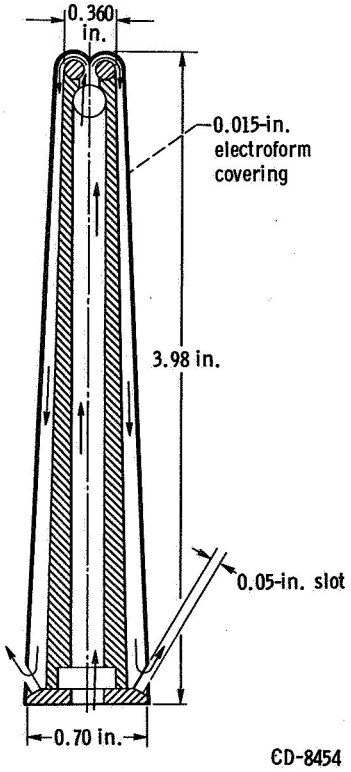

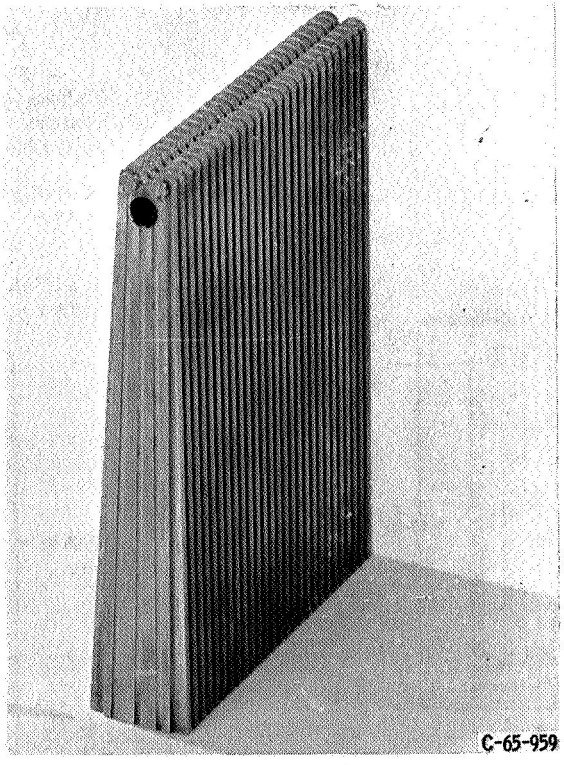

Strut before electroform covering

(c) Reverse flow convectively cooled; baffles 14 and 21.

Figure 8. - Cross-sectional views of baffles.

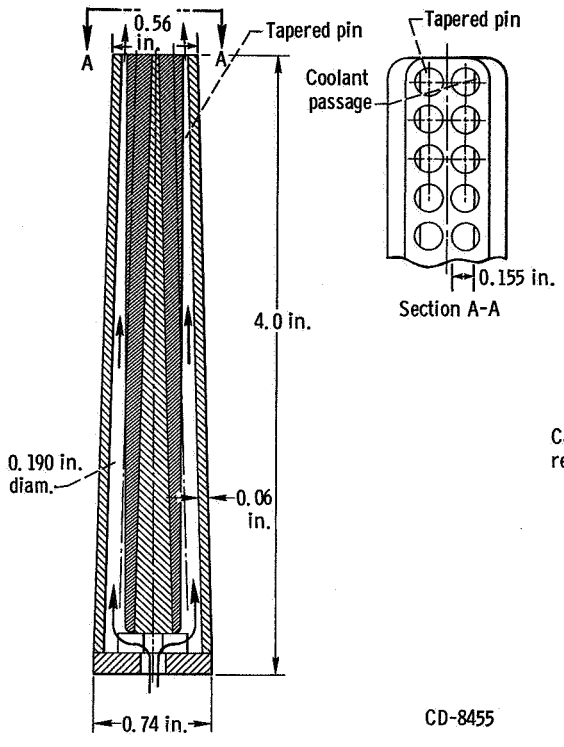

(d) Convectively cooled; baffles 10, 13, and 13M.

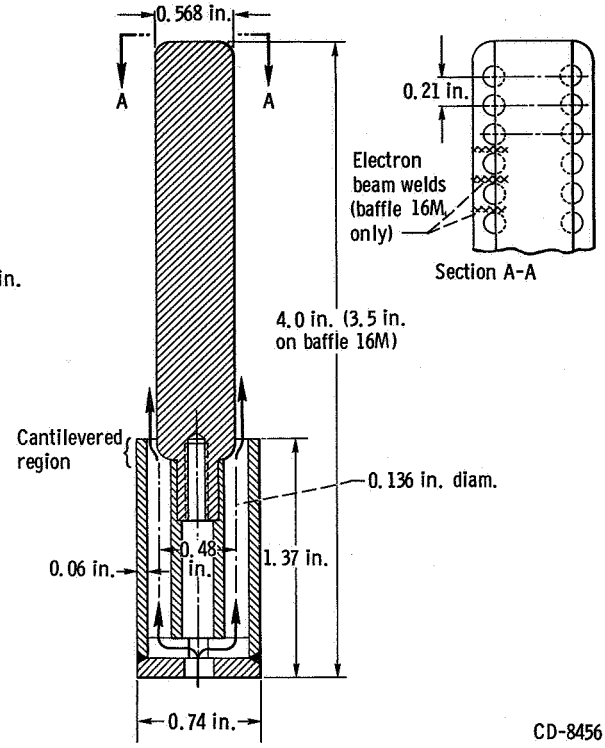

(e) Film cooled; baffles 16 and 16M.

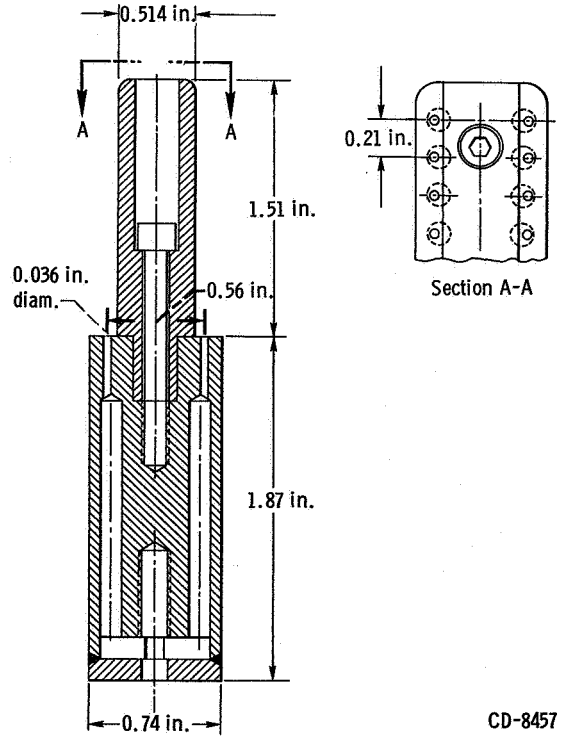

(f) Film cooled; baffle 17.

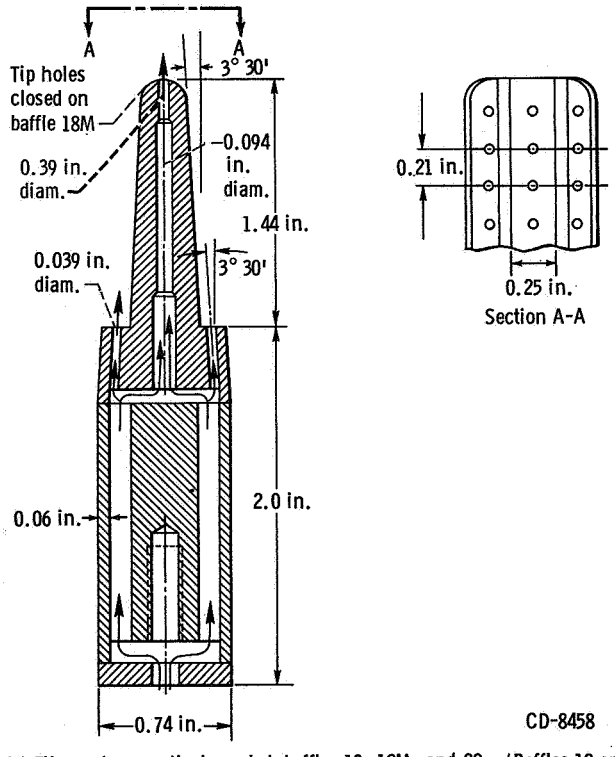

(g) Film and convectively cooled; baffles 18, 18M, and 22. (Baffles 18 and 22 are identical.)

Figure 8. - Continued.

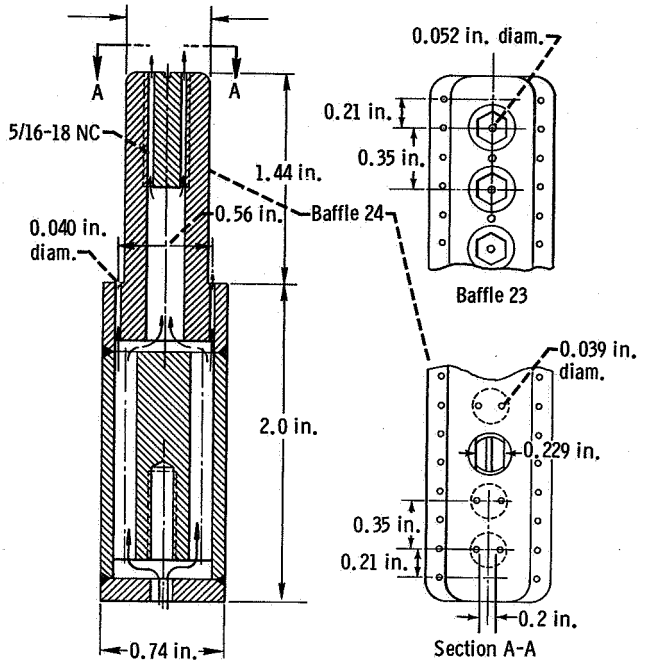

(h) Film and convectively cooled; baffles 23 and 24.

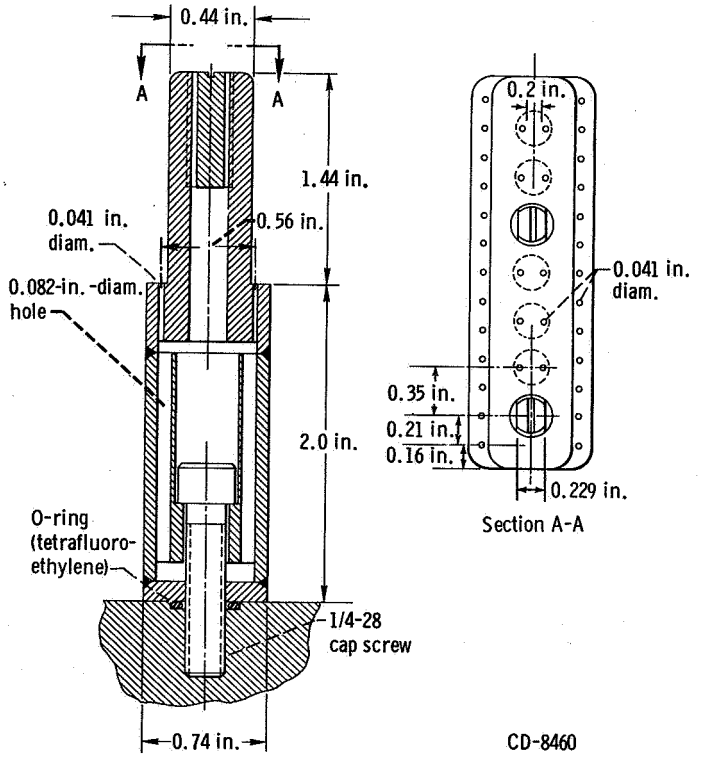

(i) Prototype film and convectively cooled; baffle 25.

Figure 8. - Concluded.

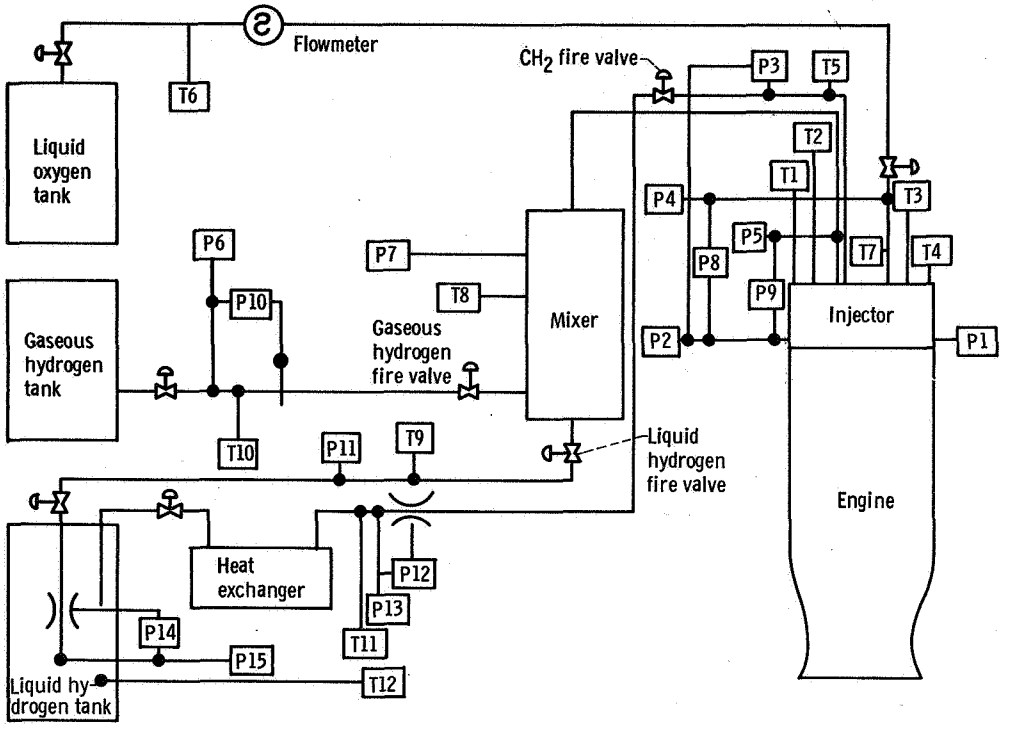

P1 Chamber pressure static (injector face), four-arm strain gage transducer 1
P2 Chamber pressure static (injector face), four-arm strain gage transducer 2
P3 Baffle differential pressure, four-arm strain gage transducer
P4 Oxygen injection pressure, four-arm strain gage transducer
P5 Hydrogen injection pressure, four-arm strain gage transducer
P6 Gaseous hydrogen orifice pressure, four-arm strain gage transducer
P7 Hydrogen mixer pressure, four-arm strain gage transducer
P8 Oxygen injection differential pressure, four-arm strain gage transducer
P9 Hydrogen injection differential pressure, four-arm strain gage transducer
P10 Gaseous hydrogen orifice differential pressure, four-arm strain gage transducer
P11 Liquid hydrogen line pressure, four-arm strain gage transducer
P12 Coolant hydrogen venturi differential pressure, four-arm strain gage transducer
P13 Coolant hydrogen venturi pressure, four-arm strain gage transducer
P14 Liquid hydrogen venturi differential pressure, four-arm strain gage type
P15 Liquid hydrogen venturi pressure, four-arm strain gage transducer
T1 Hydrogen injector temperature, carbon resistor sensor probe 1
T2 Hydrogen injector temperature, carbon resistor sensor probe 2
T3 Hydrogen injector temperature, carbon resistor sensor probe 3
T4 Hydrogen injector temperature, carbon resistor sensor probe 4
T5 Baffle inlet temperature, carbon resistor sensor probe
T6 Oxygen flowmeter temperature, platinum type
T7 Oxygen injection temperature, copper-constantan thermocouple
T8 Hydrogen mixer temperature, carbon resistor sensor probe
T9 Liquid hydrogen line temperature, carbon resistor sensor probe
T10 Gaseous hydrogen orifice temperature, iron-constantan thermocouple
T11 Coolant hydrogen venturi temperature, carbon resistor sensor probe
T12 Liquid hydrogen venturi temperature, platinum type

Figure 9. - Instrumentation diagram.

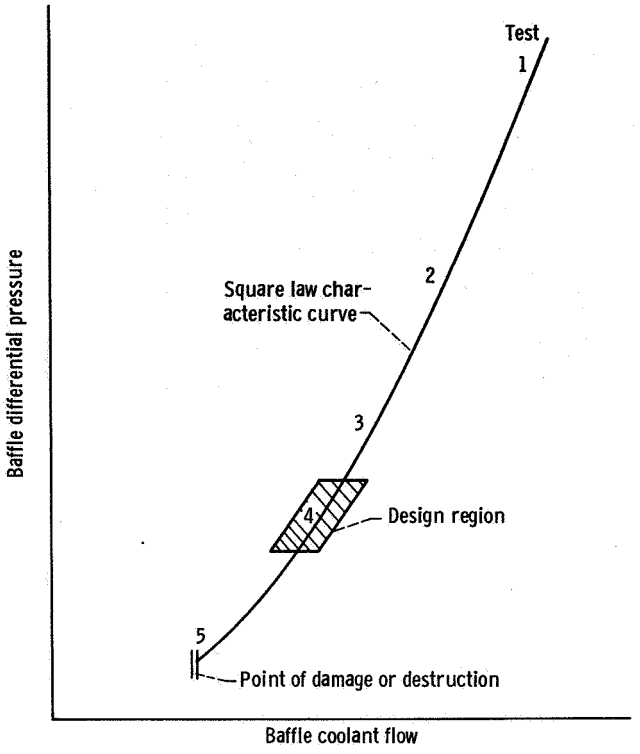

Figure 10. - Anticipated form of test results.

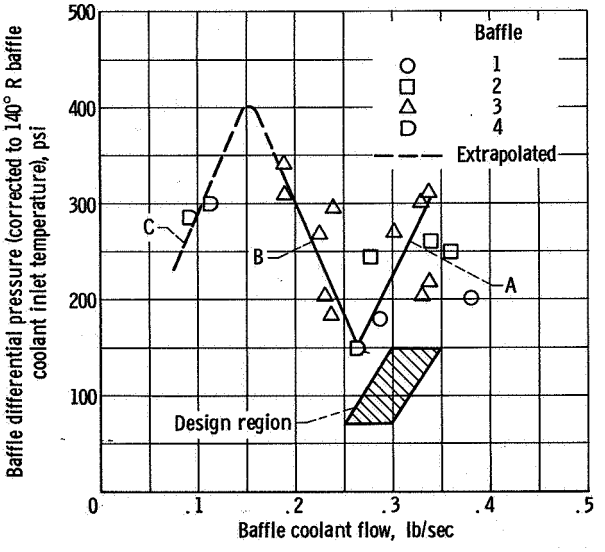

Figure 11. - Flow characteristics of transpiration cooled baffles; baffles 1, 2, 3, and 4.

C-65-1511

Figure 12. - Damage to transpiration cooled baffle 4.

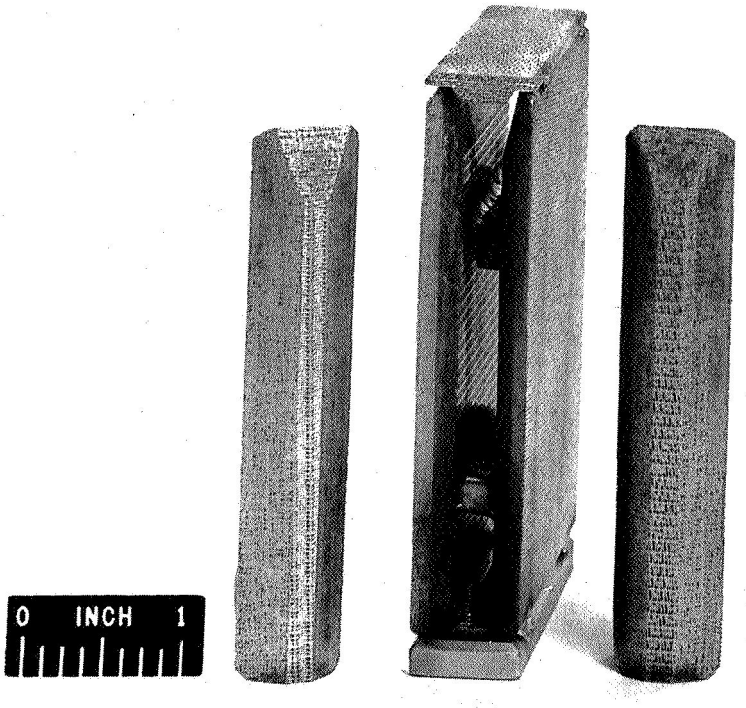

C-65-541

Figure 13. - Transpiration cooled baffle prior to welding.

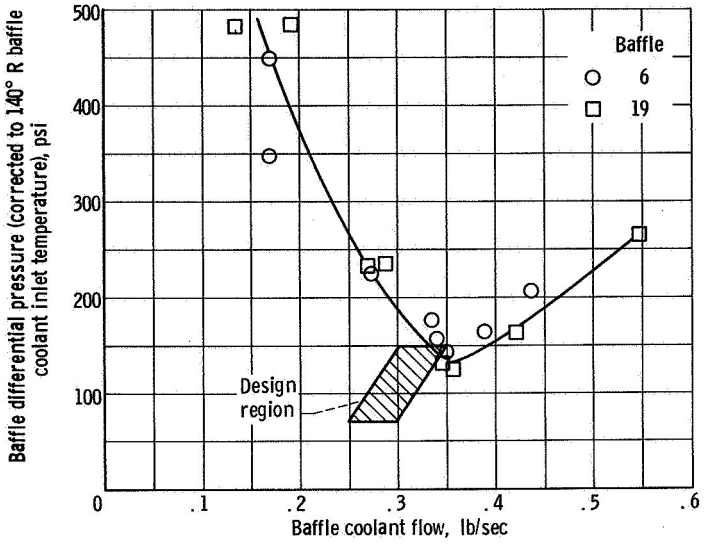

Figure 14. - Flow characteristics of transpiration cooled baffles; baffles 6 and 19.

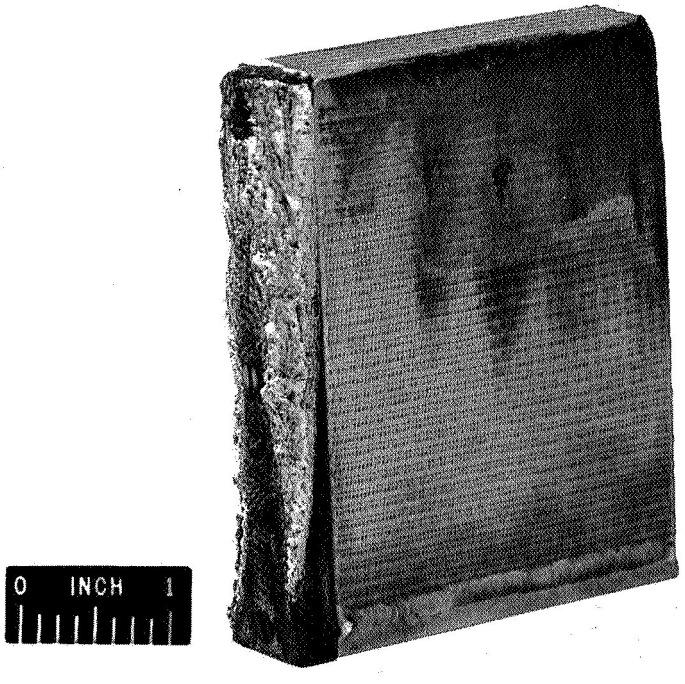

C-65-1728

Figure 15. - Postfire condition of transpiration cooled baffle; baffle 6.

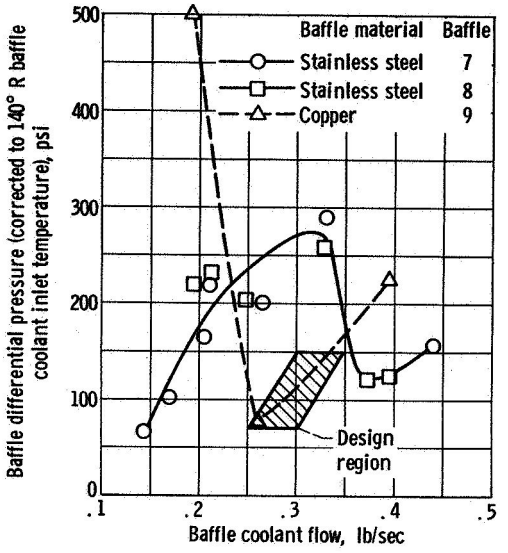

Figure 16. - Flow characteristics of transpiration cooled baffles using two layers of thin porous material.

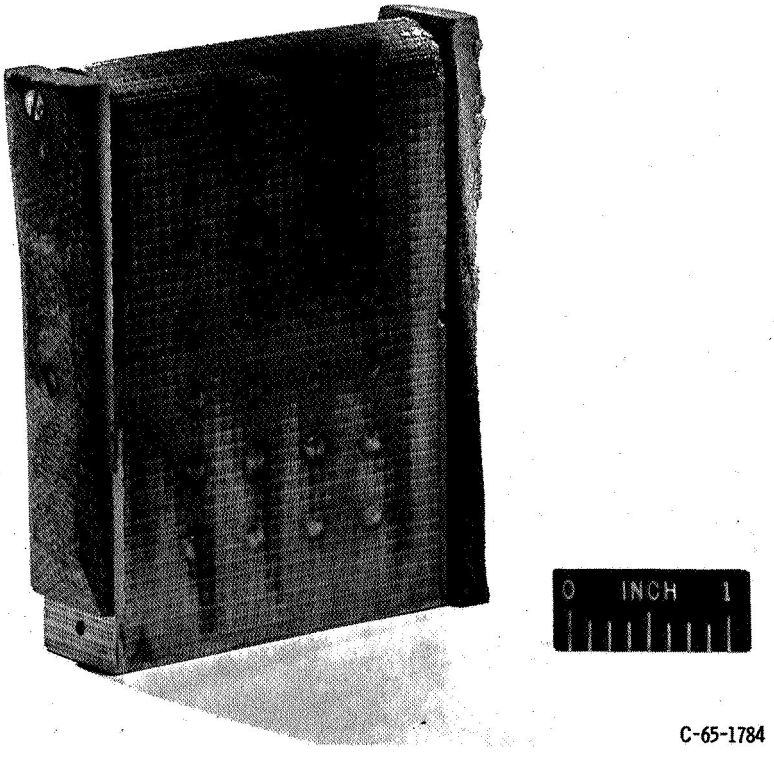

C-65-1784

Figure 17. - Postfire condition of baffle 7.

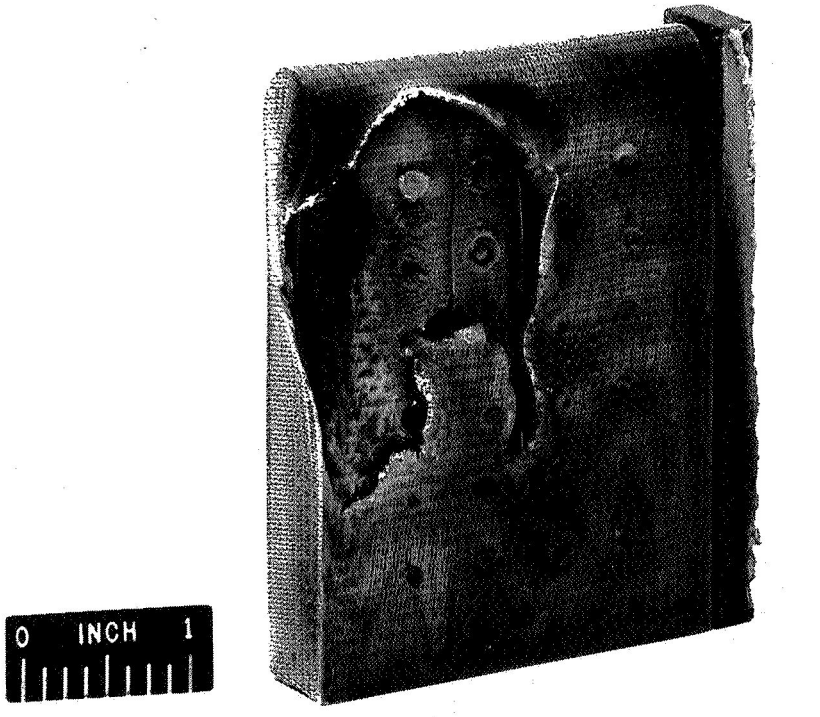

C-65-1733

Figure 18. - Postfire condition of baffle 9.

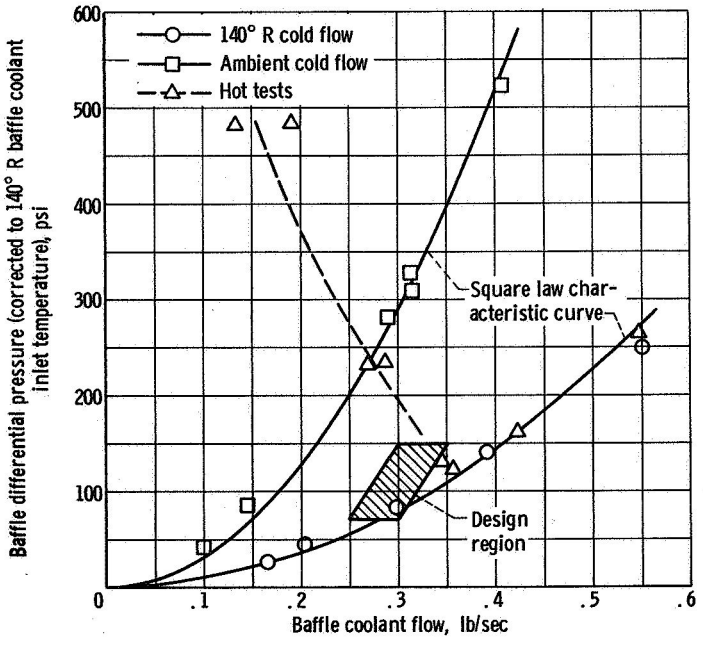

Figure 19. - Comparison of firing and nonfiring flow characteristics of transpiration cooled baffle 19.

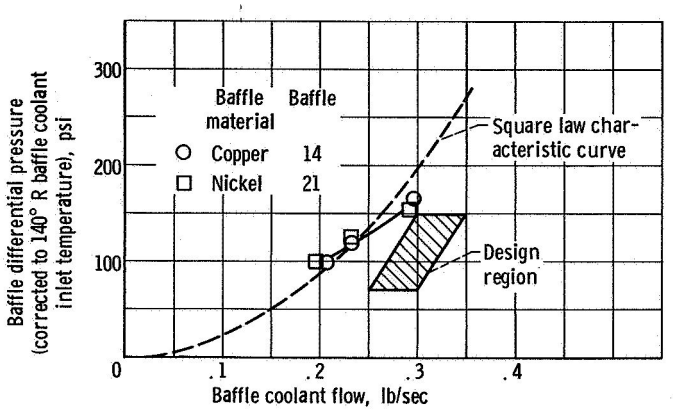

Figure 20. - Flow characteristics of reverse flow baffles 14 and 21.

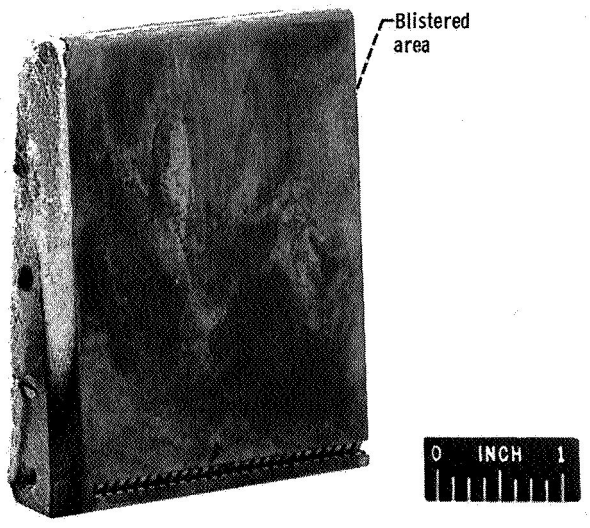

C-65-1787

(a) Copper baffle 14.

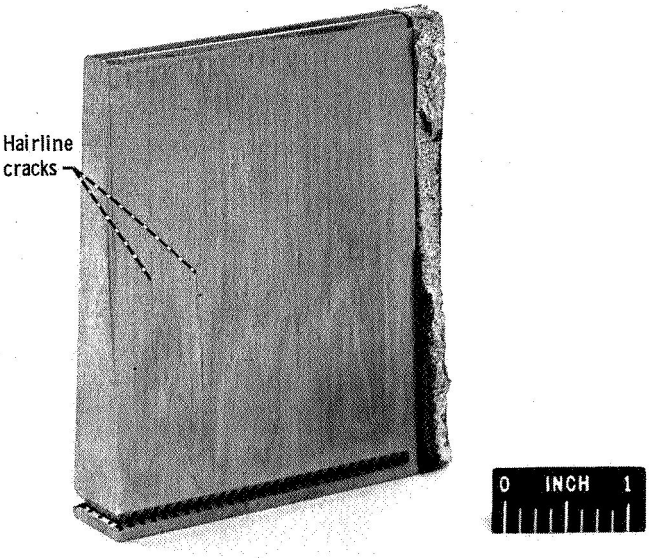

C-65-2452

(b) Nickel baffle 21.

Figure 21. - Postfire condition of reverse-flow baffles 14 and 21.

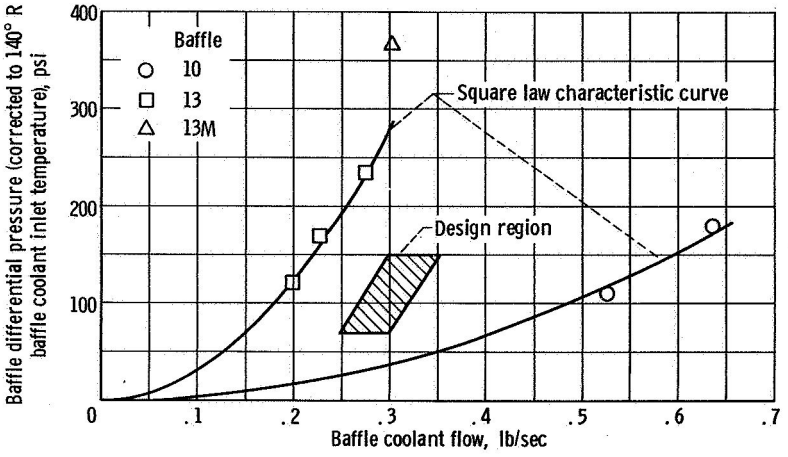

Figure 22. - Flow characteristics of the dump cooled baffles.

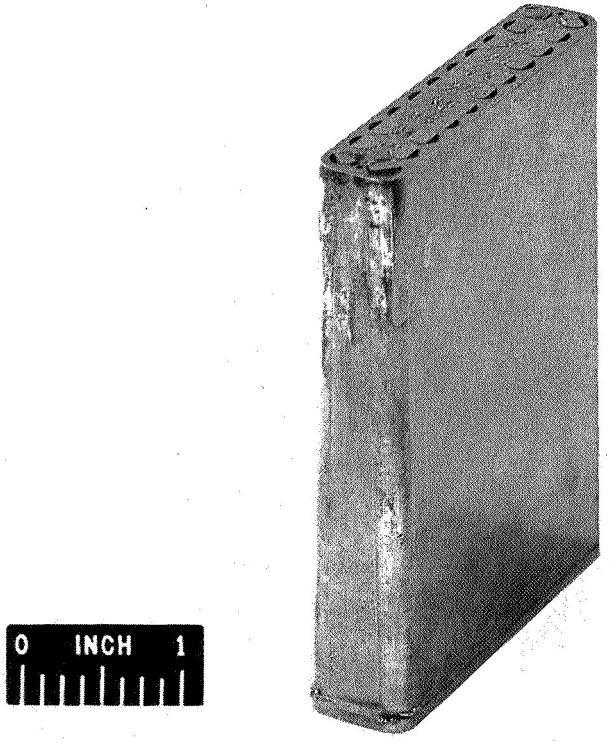

C-65-957

Figure 23. - Postfire condition of baffle 10.

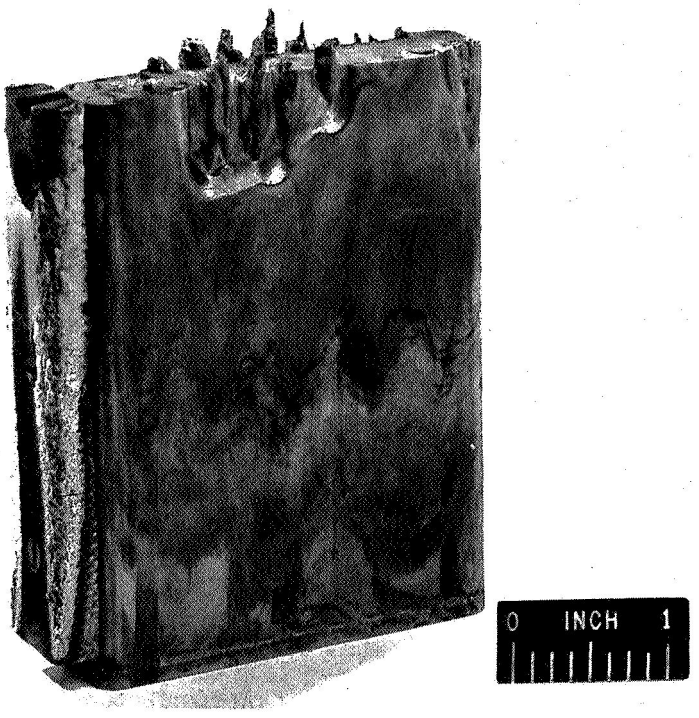

C-65-2061

Figure 24. - Postfire condition of baffle 13 after operation at about 75 percent of design coolant flow.

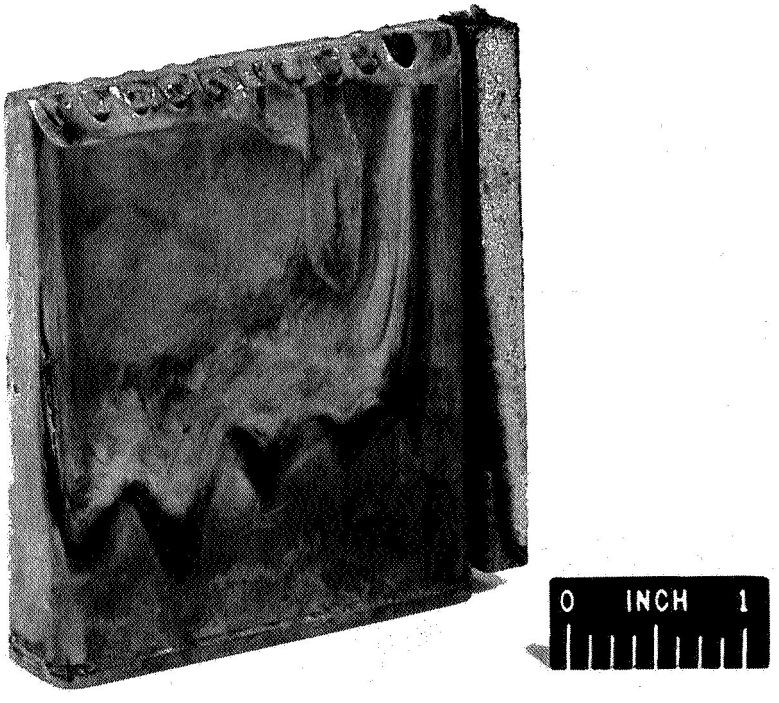

C-65-2202

Figure 25. - Postfire condition of baffle 13M.

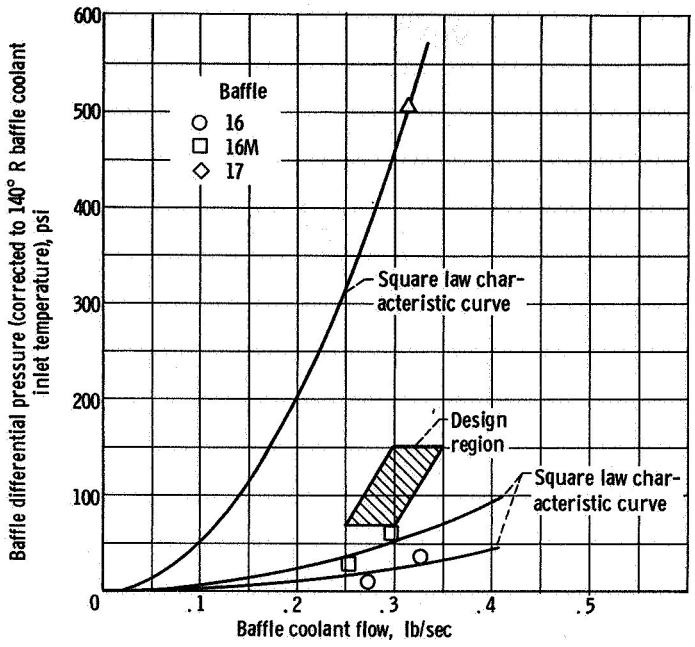

Figure 26. - Flow characteristics of film cooled baffles 16, 16M, and 17.

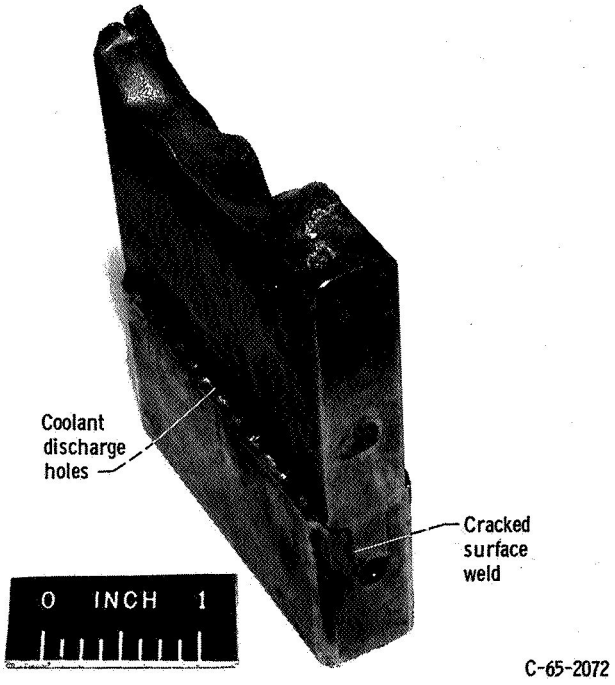

Figure 27. - Postfire condition of baffle 16M.

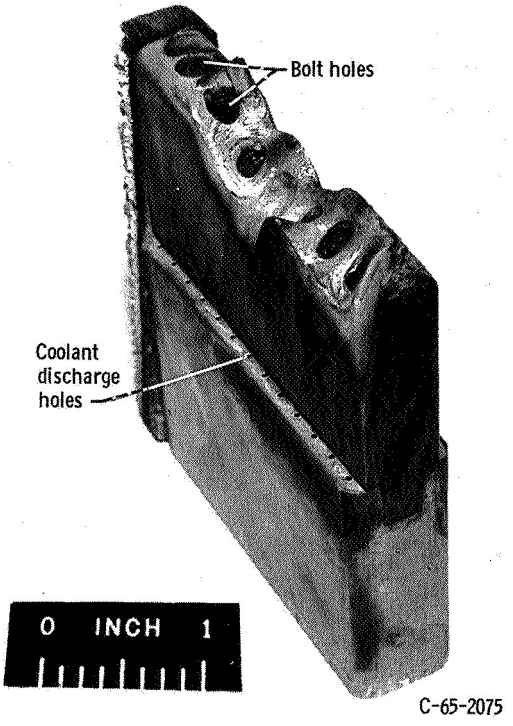

Figure 28. - Postfire condition of baffle 17.

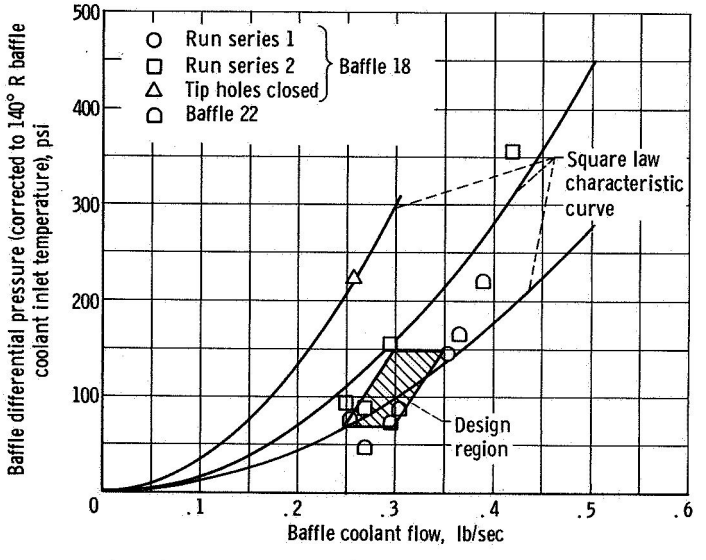

Figure 29. - Flow characteristics of baffles 18, 18M, and 22 which used combined film and dump cooling.

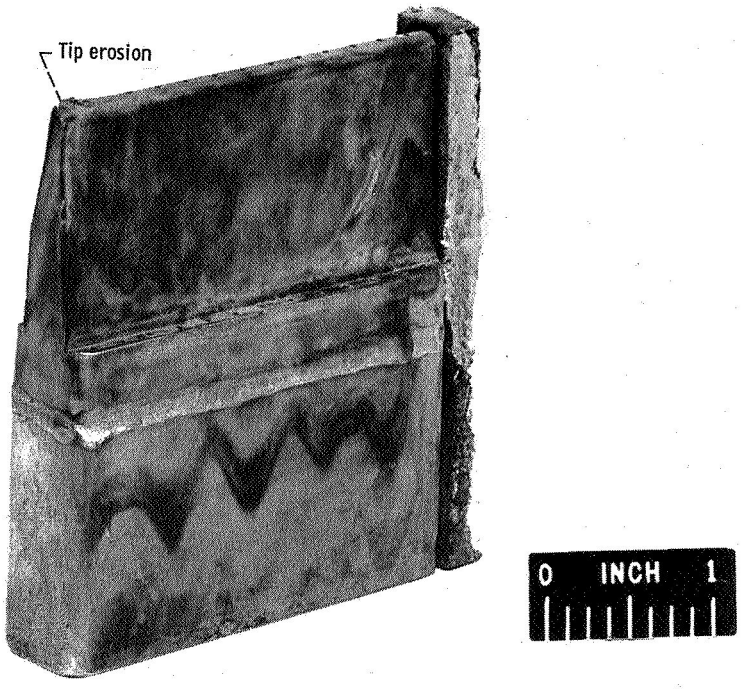

C-65-2193

Figure 30. - Postfire condition of baffle 18.

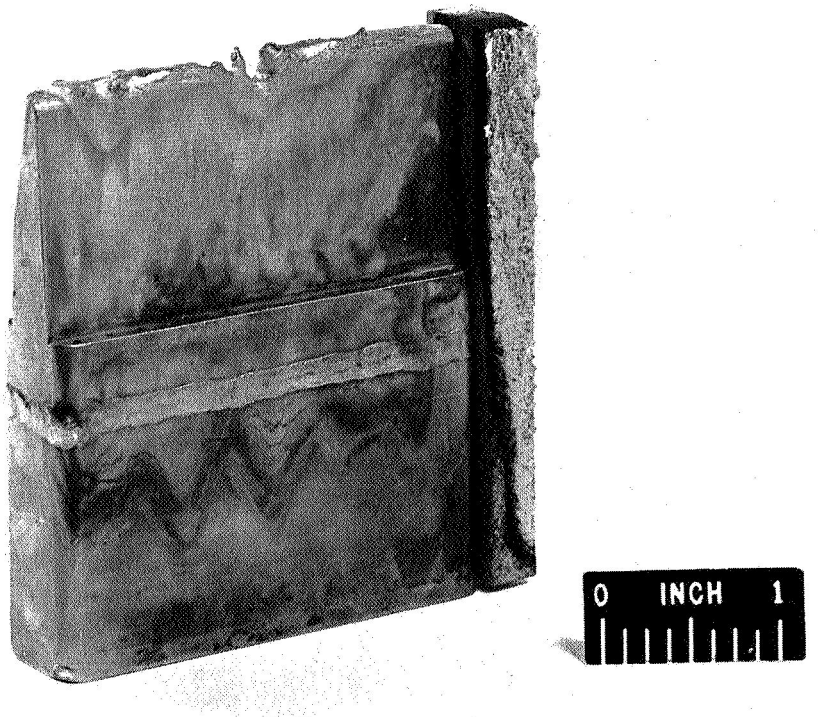

C-65-2199

Figure 31. - Postfire condition of baffle 18M.

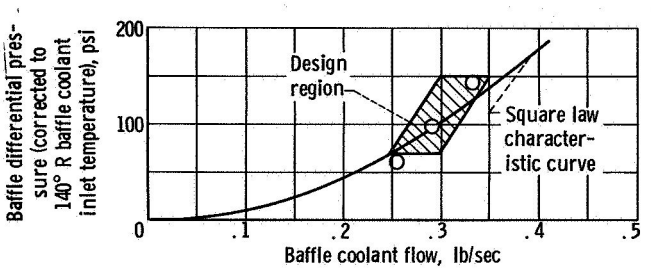

Figure 32. - Flow characteristics of baffle 23.

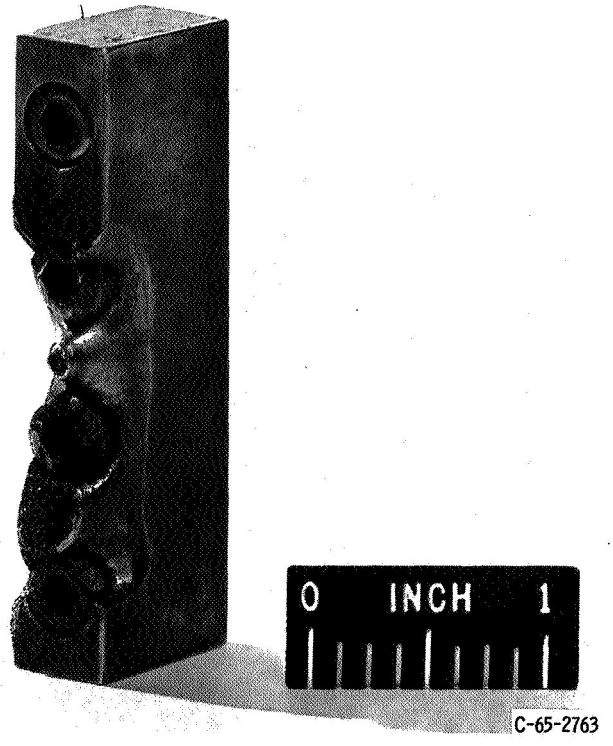

Figure 33. - Postfire condition of tip section of baffle 23.

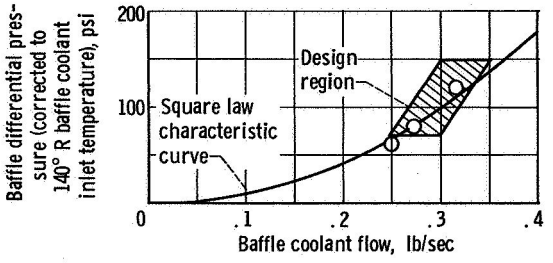

Figure 34. - Flow characteristics of baffle 24.

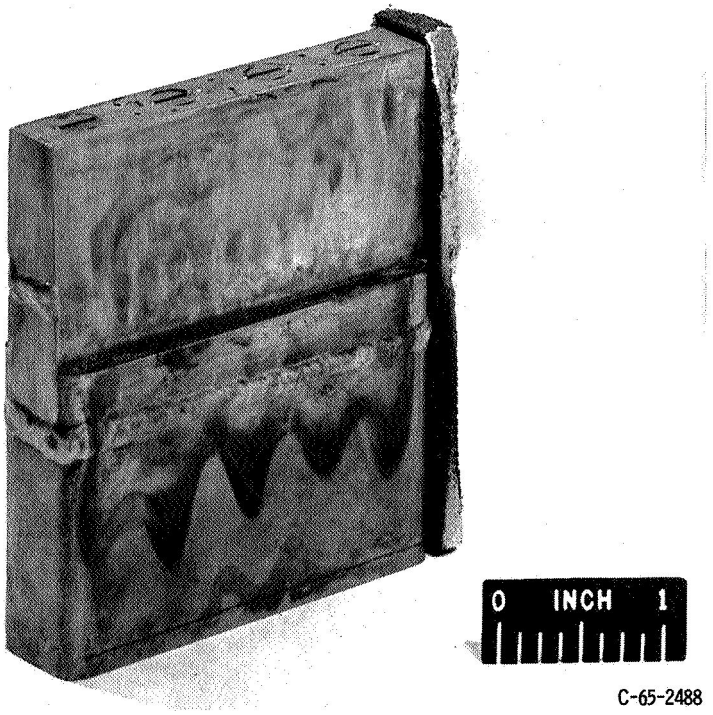

Figure 35. - Postfire condition of baffle 24.

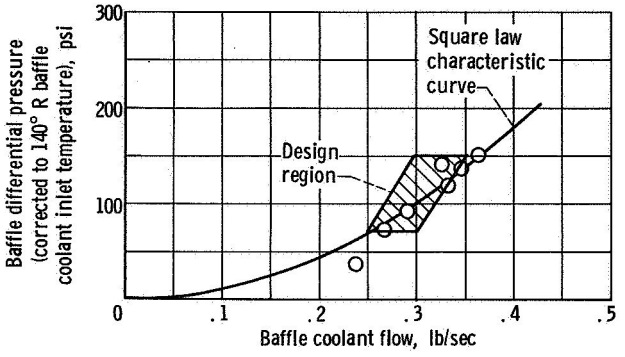

Figure 36. - Flow characteristics of prototype baffle (baffle 25).

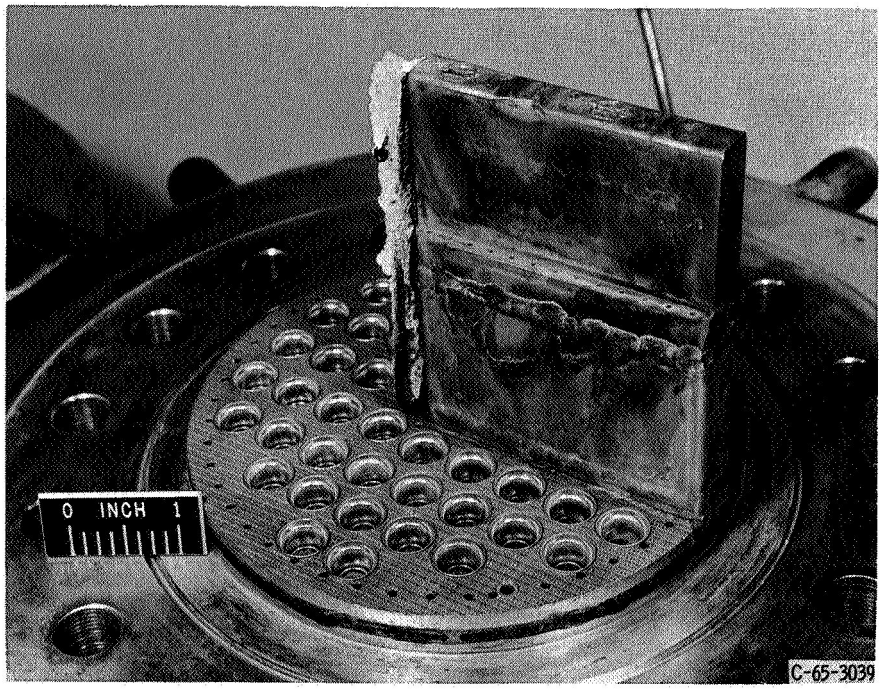

Figure 37. - Postfire condition of baffle 25 after 10 seconds of operation at lower limit of design coolant flow.

Figure 38. - Postfire condition of baffle 25 after 10 seconds of operation at 80 percent of lower limit of design coolant flow.

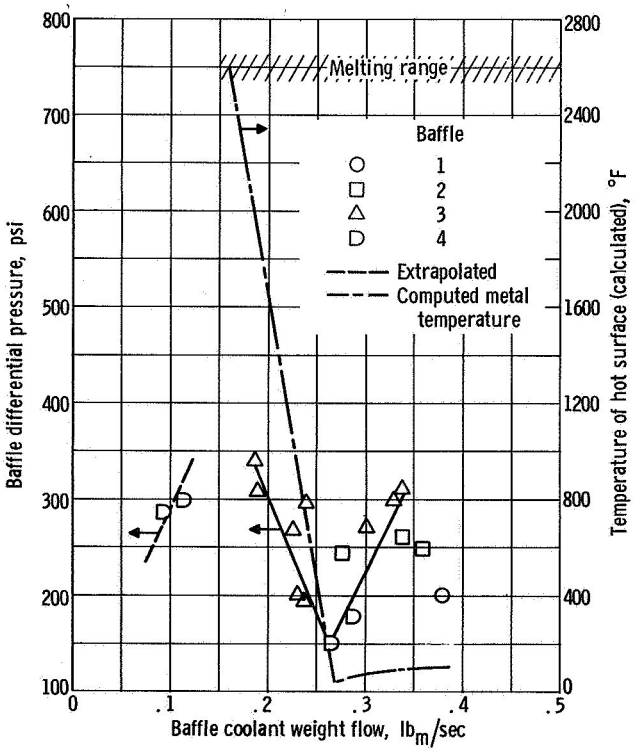

Figure 39. - Flow characteristics of transpiration cooled baffle with computed metal temperature.